Performance comparison of resin-infused thermoplastic and thermoset 3D fabric composites under impact loading

S.Z.H. Shah , P.S.M. Megat-Yusoff , S. Karuppanan , R.S. Choudhry , F. Ahmad , Z. Sajid , P. Gerard , K. Sharp

PII: S0020-7403(20)32723-5
DOI: https://doi.org/10.1016/j.ijmecsci.2020.105984
Reference: MS 105984

To appear in: *International Journal of Mechanical Sciences*

Received date: 20 June 2020
Revised date: 27 July 2020
Accepted date: 28 July 2020

Please cite this article as: S.Z.H. Shah , P.S.M. Megat-Yusoff , S. Karuppanan , R.S. Choudhry , F. Ahmad , Z. Sajid , P. Gerard , K. Sharp , Performance comparison of resin-infused thermoplastic and thermoset 3D fabric composites under impact loading, *International Journal of Mechanical Sciences* (2020), doi: https://doi.org/10.1016/j.ijmecsci.2020.105984

Highlight

- The fabrication of 3D composite with a thermoplastic and thermoset matrix using a vacuum infusion process.
- Single and recurring low-velocity impact responses of resin-infused thermoplastic and thermoset 3D composites were investigated.
- The damage mechanisms of the thermoplastic 3D composite were explored under low-velocity impact and compared with conventional thermoset 3D composite.
- The effect of resin toughness on the low-velocity impact performance of 3D composites was studied.
- Damage accumulation in 3D composites under recurring impact was explored.

Performance comparison of resin-infused thermoplastic and thermoset 3D fabric composites under impact loading

S.Z.H. Shah [a], P.S.M. Megat-Yusoff [b,*], S. Karuppanan [c], R.S. Choudhry [d]
F. Ahmad [e], Z. Sajid [f], P. Gerard [g], K. Sharp [h]

[a,b,c,e,f] *Department of Mechanical Engineering, Universiti Teknologi PETRONAS, 32610 Bandar Seri Iskandar, Perak, Malaysia*
[d] *Department of Mechanical and Manufacturing Engineering, University of Derby, UK*
[g] *ARKEMA, Groupement de Recherche de Lacq, F-64170 Lacq, France*
[h] *TexTech Industries, Inc., 1 City Center, Portland, ME, 04101, USA*
**Corresponding author: puteris@utp.edu.my, Tel: +6053687149*

Abstract

In this paper, the impact performance of a novel resin-infused acrylic thermoplastic matrix-based 3D glass fabric composite (3D-FRC) has been evaluated and compared with thermoset based 3D-FRC under single as well as recurring strike low velocity impact (LVI) events. The single impact tests revealed that the thermoplastic-based 3D-FRC exhibits up to 45% reduced damage area and can have up to 20% higher impact load-bearing capacity (peak force). The damage mode characterization showed that damage transition energy required for micro to macro damage transition is 27% higher, and back face damage extension is up to 3 times less for thermoplastic-based 3D-FRC. Meanwhile, the recurring strike impact test highlights that the thermoplastic-based 3D-FRC experiences a 50% less damaged area, better structural integrity, and survived more strikes. The comparison of single and repeated LVI tests have also allowed us to present a design criterion for estimating the safe number of repeated LVI events for a given impact energy. The superior impact resistance of thermoplastic-based 3D-FRC is attributed to their higher interlaminar fracture toughness, a tougher fiber-matrix interface, matrix ductility, and unique failure mechanism of yarn straining, which is not present in thermoset composites.

Keywords: 3-Dimensional reinforcement, impact behavior, thermoplastic resin, thermoset resin.

1. Introduction

One major concern for the aerospace application of fiber-reinforced composites (FRC) is their sensitivity to the low-velocity impact (LVI). This type of impact can introduce internal damage in the form of delamination, matrix cracking, and fiber failure while leaving a small or no indentation on the surface [1, 2]. These internal damage mechanisms are difficult to detect, and the extent of the internal damage is not clear from the barely visible surface damage, often requiring specialized techniques such as ultrasonic C-scans or X-ray tomography for a detailed assessment [1, 3-5]. In addition to the single impact events, during routine maintenance or in-service conditions, aerospace structures may encounter recurring impact events in a localized area [6-8]. It is evident that impact-induced damage mechanisms can grow under cyclic loads, leading to a decrease in the damage tolerance of FRC by more than 50% [9, 10]. Similarly, under compressive loading, damage caused by an impact event may initiate premature sub-laminate buckling at significantly lower loads as compared to the undamaged laminates. The problem is further complicated by the fact that reliable estimates of the reduction in strength are hard to achieve [11, 12]. Therefore, it is vital to enhance the impact resistance of FRC.

Several studies have been reported in which the fabric architecture is altered [13-19], and a toughened resin system is utilized to improve the impact resistance of FRC [5, 20-23]. As discussed extensively in [24], the fabric architecture plays a significant role in enhancing the impact resistance. Particularly, for low-velocity impact, laminates

reinforced with unidirectional fabric or 2D (planar) weaves are prone to delamination. In order to overcome this, 3D-FRCs were developed [25]. Their unique characteristic of through-the-thickness reinforcement suppresses damage (delamination) caused by LVI [26, 27]. The through-thickness reinforcement not only increases the delamination resistance and structural stability but also enhances the energy absorption capabilities due to their superior inter-laminar shear strength. Various authors studied LVI performance of 3D FRC [20, 22, 28-32] and concluded that they possess higher impact resistance and energy absorption capabilities as compared to 2D FRC. In the aerospace industry, 3D-FRC are potential structural materials for primary fuselage frame, leading edges of the wings, engine mounts, etc. [33, 34].

In addition to fabric architecture, resin toughness also plays a significant role in improving the impact resistance of FRC. In particular, the thermoplastic resin systems possess a higher strain to failure and fracture toughness than thermoset resin systems. Each of these properties increases the impact resistance of laminated composites by reducing crack propagation, damage extension, and delamination. Several authors studied thermoset based 3D-FRC. However, a few studies are available in the literature for the thermoplastic-based 3D-FRC [20, 30]. For instance, Bandaru et al. [20] explored the impact properties of polypropylene-based 3D-FRC and found that 3D-FRC absorbed 26% more impact energy as compared to 2D-FRCs. Zhang et al. [30] studied polyethylene-based 2D and 3D-FRC and reported that thermoplastic-based 3D-FRC possesses the highest impact resistance. However, in these studies, thermoplastic-based 3D-FRC were fabricated through a hot compression molding process using polypropylene films. The authors identified poor interface properties, and the 3D fabric used was only 1.2 mm thick; therefore, the impact performance and damage mechanisms of thermoplastic-based 3D-FRC are still unclear.

To date, 3D-FRC's for aerospace application are primarily manufactured through thermoset resin, employing a liquid composite molding [34] process. This is due to the reason that manufacturing of thermoplastic-based 3D-FRC using conventional techniques such as press-curing or injection molding, poses a number of challenges. Firstly, the thickness of 3D fabric can be substantial, with lamina thickness of up to 23 mm being reported in the literature for a single layer of 3D fabric. For such thick composites, low molding temperature leads to the poor wet-out and dry regions; whereas, high temperature can degrade resin and fiber properties [35]. Secondly, the hot compression molding process applies pressure only in one direction, which restricts the fabrication of complex 3D fabric architectures, i.e., near net shape designs, which is the main advantage of 3D-FRC. Thirdly, for large parts, such as wind turbine blades, large ship hulls, and aerospace structures, which usually require low to medium production volumes, these manufacturing methods become uneconomical. Processes such as vacuum-assisted resin infusion (VARI) are more economical in such cases. Finally, these processes require careful consideration of process parameters, i.e., molding temperature, molding pressure, consolidation time, among others, which significantly increases the void content in the final part [36], and degrade the performance of aerospace structures.

To overcome these difficulties an acrylic thermoplastic resin system, i.e., Elium® was developed [37]. This resin system is claimed to be the first thermoplastic resin liquid at room temperature and, due to its low viscosity, can be used for the manufacturing of 3D-FRC using conventional processes such as VARI and resin transfer molding (RTM). This opens the possibility of fabricating thick, complex, and near net-shaped thermoplastic-based 3D composite, which is easier to repair and recycle. The use of this resin system in aerospace and other structurally critical applications, however, require tight control over void content and excellent interface properties, which will increase the reliability. It is, therefore, important to fully establish the achievable properties from this new resin system and to have a thorough comparison against other established candidates. In recent years, some authors [38-40] have evaluated the tensile,

compression, shear, and impact properties of the non-crimp fabric, bi-directional woven fabric and flax fibers with Elium® resin. However, to the best of the authors' knowledge, impact properties of the novel thermoplastic matrix (Elium®) with 3D FRC, under single and recurring strike impact, have not been studied.

A critical novel aspect of the current work is that, no previous study carried out a detailed characterization of the failure mechanisms and the comparison of the damage development process of resin infused thermoplastic and thermoset 3D-FRC. Such a comparison is pertinent, both from the point of view of developing an academic understanding of a new resin system as well as from a practical point of view of informing the wider industry. Thus, following these directions, the present investigation aims to elucidate the effect of resin toughness on the impact resistance and the corresponding failure mechanisms. This is done by comparing both thermoplastic (Elium) and thermoset (Epoxy) 3D-FRC under single and recurring strike impact loads. In addition, the accumulation of damage from the first strike to the complete penetration of the impactor is evaluated and compared using a suitably defined damage index. This is supplemented by a detailed macroscopic damage characterization to explain the damage modes and energy absorption mechanisms in both types of 3D-FRC. Our study has shown that the damage development process for thermoplastic based 3D-FRC is significantly different with local yielding and plasticization that leads to a phenomenon of yarn-straining that is unique to the thermoplastic 3D-FRC. These phenomena lead to much higher energy absorption and reduced damage area and indentation depth. We believe that the work presented in this paper will be very useful for further development and wider application of resin infused thermoplastic 3D-FRC. Another novel aspect of the work is that based on a comparison of the single and repeat LVI events we have presented a simple yet conservative design criterion to estimate the safe number of repeated LVI events for both type of composites.

2. Experimental procedures

2.1. Material used

The fabric used in this research work was 3D orthogonal E-glass woven fabric (3D-9871) obtained from TexTech® Industries, USA, as shown in Fig.1(a). This fabric has three warp layers and four fill layers held together by a through-thickness reinforcement, which travels along the warp direction. The cross-sectional area of a middle layer along the warp direction was twofold to maintain the same areal density and in-plane properties along with both directions (warp and fill direction), as shown in the schematic diagram in Fig.1(b). The overall thickness of a single-layered dry fabric is ~4.3 mm with an areal density of 5200 GSM. The fabric consists of 49% fibers along the warp and fill direction, and 2% fibers along the thickness direction. The fill and warp count of the 3D fabric is 1.9 PPCM and 2.8 EPCM, respectively. To study the effect of resin toughness, two different resin systems were used to fabricate 3D FRC panels, i.e., a recently developed acrylic thermoplastic liquid resin Elium® 188x0 (low reactivity) supplied by Arkema and thermoset epoxy resin system Epolam® 5015/5015 supplied by Axson. The Elium® 188x0 is an acrylic monomer, which was mixed with the peroxide catalyst to initiate the polymerization process at room temperature. The percentage of peroxide may vary between 2% (slow polymerization) to 4% (fast polymerization) depending upon the requirement. In this study, low polymerization time was used (80-100 minutes). To achieve this, the ratio of Elium® and peroxide used was 100:2.25, i.e., 2.25 grams of peroxide was mixed with 100 grams of Elium® resin. Whereas, in the case of thermoset resin, the epoxy and hardener ratio used was 100:30 by weight. The mechanical properties of Elium® and Epolam® are mentioned in Table.1. A quick look at Table 1 reveals that both resin systems have nearly identical strength and stiffness, however, the toughness of thermoplastic, Elium is more than four times that of the thermoset,

Epolam and this leads to significant differences in impact response of the two systems as will be explained in the results and discussion sections.

Table.1. Summary of mechanical properties of the thermoplastic matrix (Elium®188x0) and thermoset matrix (Epolam®5015)

Property	Elium® 188x0	Epolam® 5015/5015
Tensile strength (MPa)[a]	76	80
Tensile modulus (GPa)[a]	3.3	3.1
Elongation at failure (%)[a]	6	7
Flexural strength (MPa)[a]	130	100
Flexural modulus (GPa)[a]	3.25	2.6
Fracture toughness (kJ/m^2)[b]	0.5	0.12
Rockwell Hardness[c]	99	119
Density (g/cc)[c]	1.17	1.15

[a] Material technical datasheet, [b] Reported in literature [41], [c] In-house testing.

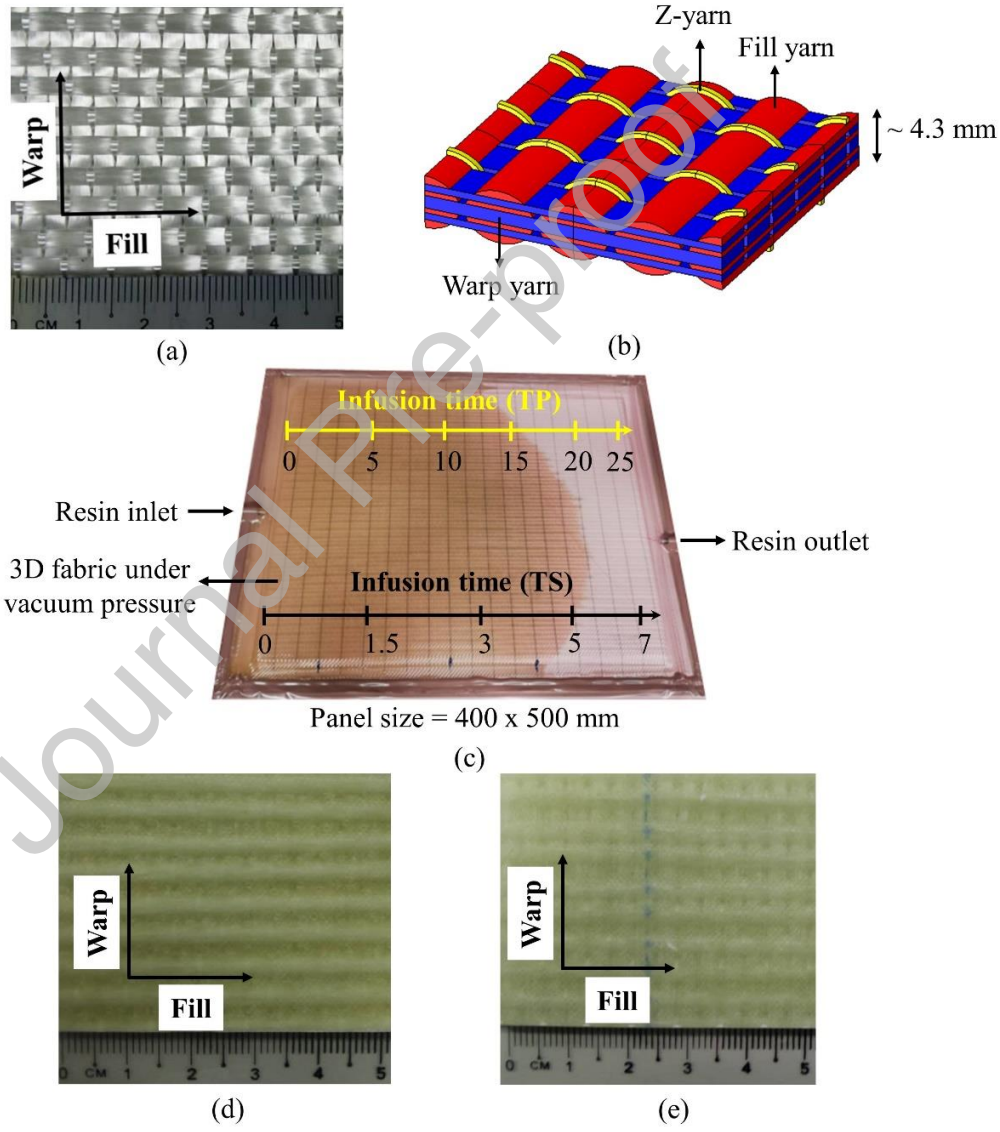

Fig.1. 3D fiber-reinforced composite and fabrication process of thermoplastic (TP) and thermoset (TS) composite. (a) 3D E-glass orthogonal woven fabric (3D-9871) used for the fabrication of 3D composites, (b) schematic diagram of 3D orthogonal fabric (blue, red and yellow colors represent warp, fill and z-yarn, respectively), (c) vacuum infusion process

along with vacuum infusion time for thermoplastic and thermoset resin (numbers marked represent resin infusion time in minutes), (d) 3D thermoplastic composite fabricated panel, and (e) 3D thermoset composite fabricated panel

2.2. Fabrication process

The vacuum-assisted resin transfer molding (VARTM) process was used to fabricate both thermoplastic and thermoset based 3D-FRC. The mixed viscosity values of Elium® 188x0 and Epolam® 5015/5015 were 200 mPa.s and 210 mPa.s, respectively, which were ideal for the VARTM process. The resin systems (Elium/peroxide and epoxy/hardener) were mixed carefully for three minutes to get a homogenous mixture. Prior to the infusion process, epoxy resin was degassed for 25 minutes to remove air bubbles, which can degrade the final mechanical properties by increasing the void contents. Since the pot life of Elium® was only 60-80 minutes, it was degassed for only 15 minutes. Somen et al. [41] highlighted the incomplete polymerization problem with Elium® 280 due to absorbed moisture and dust particles in the dry fabric. To address these problems, the infusion was carried out in a clean environment, and the 3D fabric was dried in an oven at 125 Cº for two hours prior to the infusion process. In the case of thermoplastic-based 3D-FRC, the infusion was performed at low vacuum pressure, i.e., 100 mbar to avoid resin boiling and expansion of vapors during the curing process at room temperature. The infusion was completed in 25 minutes to ensure the proper impregnation of yarns. Whereas, in the case of thermoset based 3D-FRC, the infusion was performed at 500 mbar and completed in 7 minutes, as shown in Fig.1(c). After resin infusion, the thermoplastic-based 3D-FRC panels were left at room temperature for four hours to complete the polymerization process, followed by the post-curing at 80°C for eight hours in an oven to achieve maximum mechanical properties. It is important to note that this curing time can be reduced significantly at elevated temperatures, i.e., 6 min at 80°C. Whereas, in the case of thermoset based 3D-FRC, the panels were left for twelve hours to cure at room temperature, followed by the post-curing at 80°C for eight hours.

2.3. Physical parameters of the cured panel

After the panels were fully cured, the physical parameters such as density, fiber volume fraction, and thickness of panels were measured. Fig.1. (d) and Fig.1. (e) show the fabricated thermoplastic and thermoset based 3D-FRC panels, respectively. The fiber volume fraction of the fabricated panels was measured using the burn-off method according to ASTM D3171, and the density was measured using the water displacement method according to ASTM D792-08. Ten samples were cut from different panels, and the average void content, density, and fiber volume fractions were measured, which are tabulated in Table.2. In the thermoplastic-based 3D-FRC, the void content was less than 3%; whereas, in the thermoset based 3D-FRC, the void content was less than 1%. The fiber volume fraction in both types of 3D-FRC was approximately 52%. The thickness of the fabricated panels was measured at different locations, and the average value is recorded in Table.2. The tensile strength and modulus of the thermoset based 3D-FRC along warp direction is 451 MPa and 26.3 GPa, respectively. The specimens were cut from panels using a water-based diamond tip disc cutter, which gives an excellent surface finish. Fifty-four samples were prepared for single impact tests, i.e., twenty-seven samples for each of the two material types. These were tested for nine different impact energies in the range of 10J – 100J, as detailed in Table 3. Test at each impact energy level (impact velocity) was repeated three times. Besides these samples, four samples were also prepared for recurring strike impact tests of both types of 3D-FRC.

Table.2. Physical properties of cured panels of the thermoplastic and thermoset 3D composite (each value in the table represent an average of ten samples)

Parameters	3D thermoplastic FRC	3D thermoset FRC
Thickness (mm)	4 ± 0.1	4 ± 0.1
Fiber volume fraction (%)	52 ± 1.2	52 ± 0.4
Void content (%)	2.7 ± 1	<1 ± 0.3
Density (g/cc)	1.86 ± 0.02	1.92 ± 0.01

Table.3. Low-velocity impact test parameters for a single and recurring impact test, at different impact energies. Three samples were tested at each impact energy for a single low-velocity impact test, and one sample is tested at each impact energy for a recurring low-velocity impact test.

Impact scenario	Specimen type	Impact energy (J)	Velocity (m/s)	Drop height (m)	Drop mass (kg)	No of samples
Single impact	3D-TP-FRC & 3D-TS-FRC	10	1.8	0.2	5.101	3
		15	2.4	0.3	5.101	3
		20	2.7	0.4	5.101	3
		25	3	0.5	5.101	3
		30	3.4	0.6	5.101	3
		40	3.9	0.8	5.101	3
		50	4.4	1	5.101	3
		75	5.4	1.5	5.101	3
		100	6.2	2	5.101	3
Recurring strike impact	3D-TP-FRC & 3D-TS-FRC	30	3.4	0.6	5.101	1
		50	4.4	1	5.101	1

2.4. Drop weight impact test

The impact resistance of 3D-FRC was evaluated using a drop-weight impact test, according to ASTM D7136 test protocol [42]. The experiments were performed at the Department of Mechanical Engineering, University Putra Malaysia, using an Instron® drop weight impact tower. The test setup is shown in Fig.2. The geometry of the impactor selected was cylindrical, which has a 16 mm diameter and hemispherical nose at the end. The test setup was equipped with an optical sensor to measure the initial velocity of the impactor before the impact. The impactor was instrumented with a 22.5 kN load cell to record the contact force between the impactor and composite surface. The total mass of the impactor with carriage was 5.101 kg. In all tests, the impact of energy was varied by changing the release height of the impactor. During the test, various impact parameters, i.e., specimen deflection, impact energy, impact velocity, and impact force, were determined by the data acquisition system. The flat specimen of 100 mm x 150 mm was cut from the fabricated panels. The specimen was clamped on the impact test fixture using four clamps, which has rubber dampers at the end to absorb vibrations caused by the impact. The test fixture provides a free rectangular area of 125 mm x 75 mm. The release height of the impactor was calculated using an energy conservation equation, i.e., $E = mgh$, where, E = potential energy of the impactor, h = drop weight height of the impactor, g = acceleration due to gravity and m = mass of the impactor.

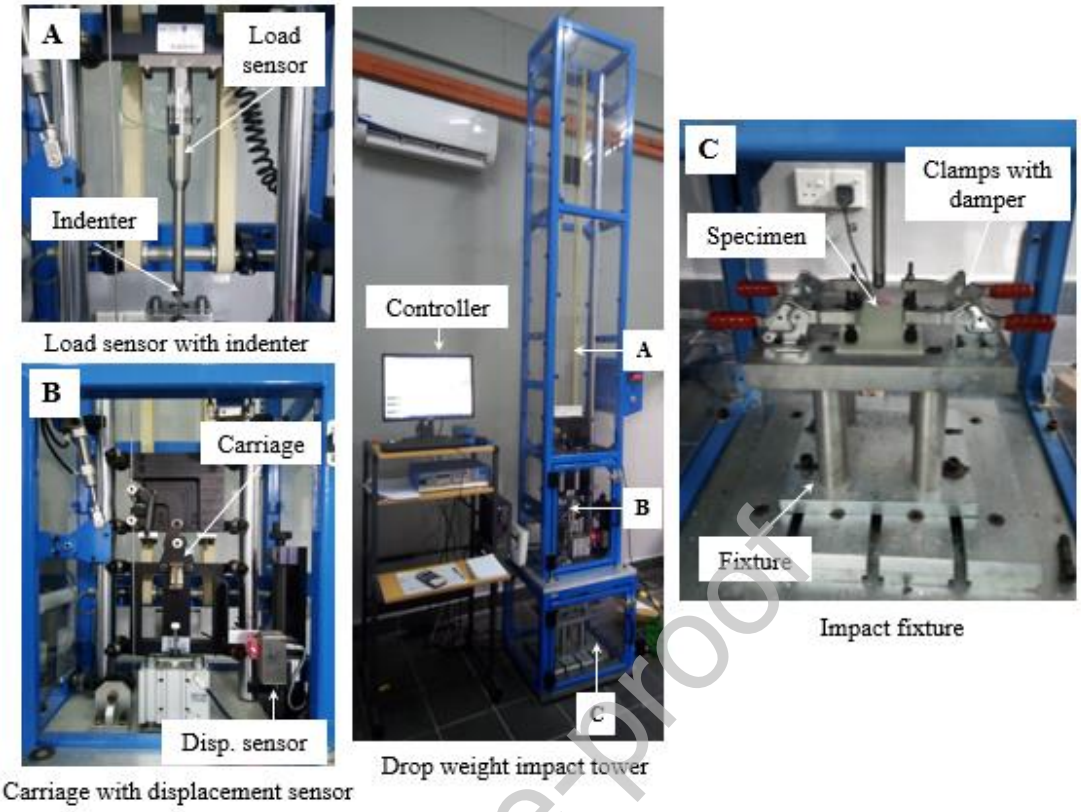

Fig.2. Drop weight impact test tower for the low-velocity impact tests of fiber-reinforced composites. The setup consists of three main sections, (A) indenter with load cell, (B) carriage with displacement sensor, and (C) fixture with clamps to hold specimen during the impact test. The clamps are equipped with rubber dampers to absorb the vibration caused by the indenter.

In the case of single impact, the low-velocity impact tests were carried out at room temperature using different impact energies ranging from 10 J ($V_{impactor} \approx 2\,m/s$) to 100 J ($V_{impactor} \approx 6\,m/s$) to study the complete behavior of 3D FRC under the low-velocity impact, i.e., rebound, penetration, and perforation. Whereas, in the case of recurring strike impact, five successive low-velocity impacts were conducted on both thermoplastic and thermoset based 3D-FRC at 30 J ($V_{impactor} \approx 3\,m/s$) and 50 J ($V_{impactor} \approx 4\,m/s$). After each strike, different parameters, i.e., impact force, displacement, velocity, elastic energy with respect to time, were recorded by the data acquisition system. Table.3. shows the impact parameters used in both strike impact tests, i.e., energies, velocities, and the drop weight height of the impactor.

2.5. Damage evaluation methods

In this study, the damaged area and permanent indentation caused by the indentor were measured to evaluate and compare the impact resistance of both thermoplastic and thermoset 3D-FRC under single and recurring strike impact. The global impact damage area of specimens was evaluated using backlight methods. The glass/epoxy and glass/Elium® are translucent under the backlight. The presence of any damage to the material reduces the translucence in the local region [6, 28]. This characteristic of glass/epoxy and glass/Elium® enables us to identify damage areas in 3D-FRC, as depicted in Fig.3(a). A similar methodology was also used by Choudhry et al. [3] to characterize impact damage in bounded joints of the woven composite. In this study, the damaged area of specimens has been evaluated using a two-step methodology. In the first step, the specimen was placed flat on a hollow cylinder containing a light

source (3" illumination ring light from TMS® LITE). The images were captured using the digital camera (Cannon Legria® 8-megapixel digital camera) from vertically above the specimen. A ruler was also placed next to the specimen, to allow for the image to be easily scaled during post-processing. In the next step, these digital images were post-processed through ImageJ software [43], to obtain damage area. The permanent indentation caused by the indentor was measured using dial gauge, as shown in Fig.3(b). The dial gauge was fixed on a stand, which can measure the permanent indentation depth up to ± 0.01 mm accuracy. It is worth noting that the indentation just after the impact is always greater and required relaxation time to eliminate such effects [44]. In this study, the indentations were measured after 48 hours of relaxation time using a dial gauge.

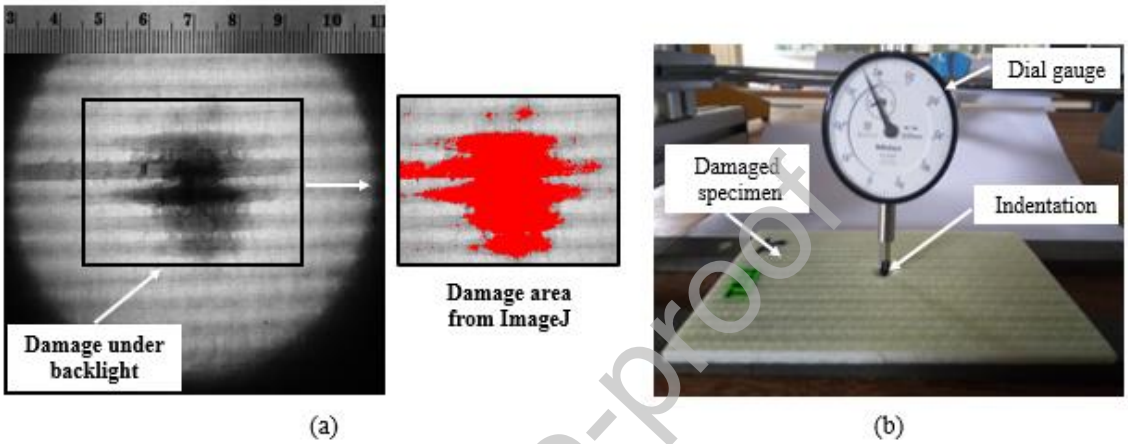

Fig.3. Damage evaluation in 3D composites after drop weight impact test, (a) damage area under backlight and through ImageJ software (red color represents damage area obtained after post-processing of backlight images in ImageJ software) (b) setup used for the measurement of permanent indentation depth using a dial gauge.

2.6. Damage accumulation under recurring strikes

The performance of thermoplastic and thermoset based 3D-FRC was evaluated after each recurring strike based on the damage variable. The damage variable indicates the accumulation of damage from the first strike to the complete penetration of the impactor. Belingardi et al. [45] proposed a damage index for thick laminates under the recurring impact. The authors monitored damage state through normalized maximum displacement and the ratio of absorbed/impact energy. The proposed damage index increases non-monotonically, which makes it difficult to characterize damage accumulation. Recently, the damage index was modified by Liao et al. [46] to determine damage accumulation in thick laminates under recurring strikes. The new damage variable is based on the bending stiffness reduction ratio, "K_r" instead of energy ratio (absorbed/impact energy ratio) and normalized maximum displacement "d_{max}", given by Eqn. (1). The modified damage variable (DI - B) increases monotonically from 0 (no damage) to 1 (complete penetration).

$$Damage\ variable\ = DI - B = K_r \times d_{max} = \left(\frac{k_1 - k_i}{k_1 - k_f}\right) \times \frac{d_i}{d_f} \quad (1)$$

where *"d_i"* and *"d_f"* represent the maximum central deflection and deflection at the penetration of the impactor, obtained from the force-deflection curve. "k_1", "k_f" and "k_i" represent bending stiffness at first strike, bending stiffness at penetration and bending stiffness at *"i^{th}"* strike.

3. Results

3.1. Single impact test

In this section, the impact performance of thermoplastic and thermoset based 3D-FRCs are evaluated and compared in terms of force-displacement, force-time, energy-time, energy profile diagram and impact resistance (permanent indentation and damaged area) due to single impact event. In addition to this, a detailed macroscopic damage characterization was performed to determined damage propagation and energy absorption mechanisms in both types of 3D-FRCs.

3.1.1. Force-displacement, energy-time and force-time response

The force-displacement curve gives bending stiffness, maximum displacement and damage occurred at different incident energies. Fig.4. depicts the force-displacement curves of 3D-FRCs at different low (25 J and 50 J) and medium (75 J and 100 J) impact energies. The force-displacement curves also show the damage process in FRC [1, 47]. In the LVI event, the kinetic energy of the indentor is transferred to the specimen in the form of elastic energy. The contact force increases until it reached a maximum value, i.e. "F_{max}", where the impactor is completely stopped, as shown in Fig.4. During this process, some of the energy is absorbed (dissipated energy during the impact) by the material, and the remaining elastic energy (non-dissipated energy during the impact) is consumed to rebound the impactor, which is indicated by the decrease in the force in the force-displacement curve. The thermoplastic-based 3D-FRC exhibited closed curves at all impact energies due to the rebound of impactor; whereas, the thermoset based 3D-FRC exhibited open curve at higher incident energies, indicating a complete perforation.

The slope of the force-displacement curves from these tests represents the bending stiffness or dynamic modulus of the material, which for many polymers, is loading rate-dependent [48]. The change in this slope during a test indicates damage transition and propagation in the specimen. At low impact energy (25 J), the thermoplastic-based 3D-FRC shows slightly higher deflection and lower bending stiffness, as compared to thermoset based 3D-FRC, see Fig.4(a). At 50 J, the thermoset based 3D-FRC undergoes a gradual load drop (indicating major damage) after reaching the peak force (F_{max}= 9.4 kN). The corresponding displacement at peak force is 7.7 mm. In comparison, the thermoplastic-based 3D-FRC shows a smooth unloading curve after reaching the maximum force, which indicates no major damage has occurred. The first load drop in the force-displacement curve represents the failure initiation "F_{ini}" . The thresholds for failure initiation are 3 kN (force) and 1 mm (deflection), which is almost the same for both 3D-FRC. After failure initiation, the force-displacement curves of both 3D-FRC show common features of a sawtooth profile, until it reached damage transition point *"D_t"*. At medium impact energy (75 J), the thermoplastic-based 3D-FRC showed a sudden drop (representing major damage) in the force-displacement curve after reaching the maximum peak force and the specimen undergoes the highest displacement, i.e., 11 mm, see Fig.4(c). It is worth noticing that there is a slight difference in the peak force of thermoset based 3D-FRC, as the incident energy increases from 50 J to 75 J; however, the maximum displacement increased to 12 mm due to back-face damage extension. Also, at 75J, the thermoplastic-based 3D-FRCs depict a higher peak force (12.5 kN) as compared to thermoset based 3D-FRC (10.3 kN). As the incident energy increases further (100 J), the thermoset based 3D-FRC showed complete perforation of the specimen with reduced bending stiffness, see Fig.4(d). Whereas, in the thermoplastic-based 3D-FRC, the impactor rebounds, with the remaining elastic energy and the maximum displacement recorded was 14 mm.

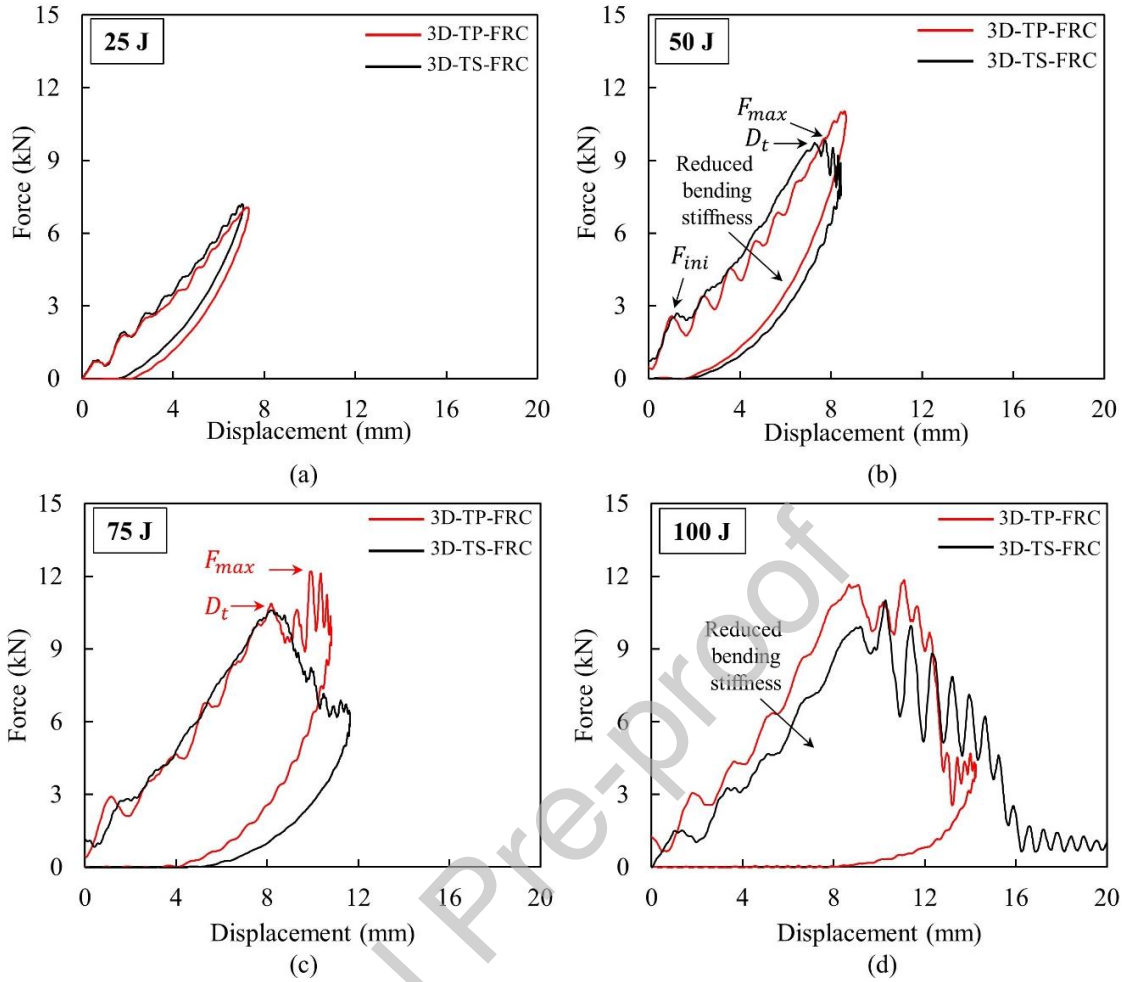

Fig.4. Comparison of single low-velocity impact response (force/displacement curves) of thermoplastic and thermoset based 3D-FRCs at different impact energies, (a) 25 J, (b) 50 J, (c) 75 J and (d) 100 J. The red and black colors represent force/displacement curves of thermoplastic and thermoset 3D composites, respectively. F_{max}, F_{ini} and D_t represent peak force, failure initiation force, and damage transition point, respectively.

The incident/impact energy is dissipated in the form of matrix cracking, fiber failure, permanent indentation, delamination, penetration, elastoplastic deformation, sound and heat, etc. Fig.5. shows the comparison between thermoplastic and thermoset based 3D-FRC in-terms of force-time and energy-time curves at different low (25 J and 50 J) and medium (75 J and 100 J) impact energies. At 25 J, both 3D-FRCs exhibited almost similar force-time response; however, the thermoplastic-based 3D-FRC showed slightly better-dissipated energy, as depicted in Fig.5(a). At 50 J, the thermoplastic and thermoset based 3D-FRC dissipated 27 J and 34 J of incident energy, whereas, at 75 J, they dissipated 55 J and 64 J of incident energy, as shown in Fig.5(b) and Fig.5(c), respectively. At 75 J, the thermoset based 3D-FRC dissipated 84% of the incident impact energy; whereas, the thermoplastic-based 3D-FRC dissipated 74% of the incident impact energy. It is important to note that at both energy levels, the dissipated energy is less than the impact energy, which indicates no penetration occurred at these stages. In terms of load-bearing capacity, the thermoplastic-based 3D-FRC showed a 20% higher peak force. At 100 J, both 3D-FRCs showed utterly different behavior. The thermoset based 3D-FRC completely perforated; whereas, in the case of thermoplastic-based 3D-FRC impactor rebounds with the remaining 8 J of elastic energy, as shown in Fig.5(d). The energy-time curve highlights that in the thermoset based 3D-FRC, perforation starts at 88 J. In terms of energy required to damage transition (micro-macro damages), the

thermoplastic-based 3D-FRCs exhibited higher damage transition energy, i.e., 44 J (Fig.5(b) as compared to 32 J (Fig.5(c)), in the case of the thermoplastic-based 3D-FRC. This indicates that the thermoplastic-based 3D-FRC possesses 27% higher damage transition energy. The summary of the single impact test results is given in Table.4.

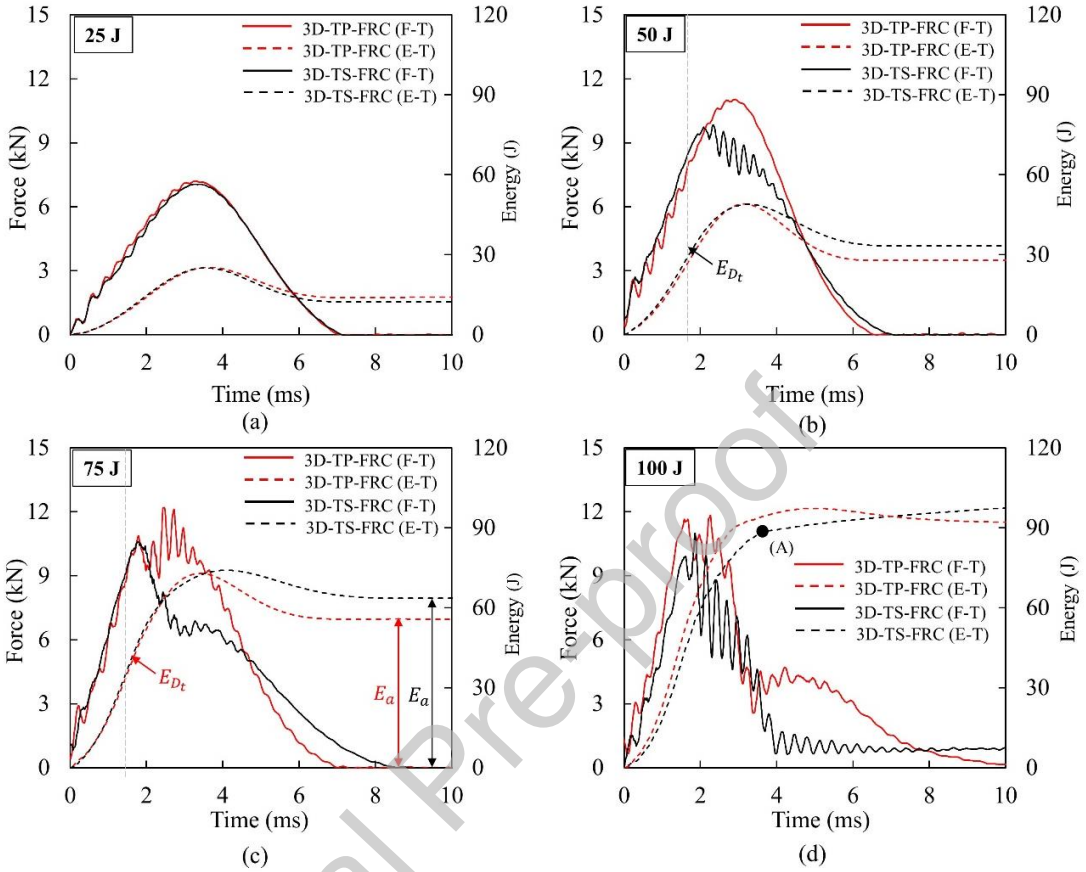

Fig.5. Comparison of single low-velocity impact response (force/time and energy/time curves) of thermoplastic and thermoset based 3D-FRCs at different impact energies (a) 25 J, (b) 50 J, (c) 75 J and (d) 100 J. The red and black colors represent the response of thermoplastic and thermoset 3D composites, respectively. The dashed line represents energy/time curves, and a solid line represents force/time curves. E_{D_t} and E_a, represents damage transition energy and absorbed energy, respectively. Point A represents the perforation point of the thermoset 3D composite at 88J.

Table.4. Summary of results for a single low-velocity impact test of thermoplastic and thermoset 3D composite at different impact energies.

Material	Impact energy (J)	Peak force (kN)	Disp. at peak force (mm)	Max. Disp. (mm)	Dissipated energy (J)
3D-TP-FRC	10	3.81 (3.0)	4.65 (3.8)	4.76 (3.8)	4.79 (6.2)
	15	4.99 (3.0)	5.63 (5.4)	5.72 (4.8)	7.43 (2.4)
	20	5.97 (1.5)	6.30 (7.2)	6.39 (6.3)	9.73 (3.5)
	25	7.10 (1.2)	7.11 (3.5)	7.31 (5.4)	12.10 (6.7)
	30	7.95 (1.4)	7.60 (6.5)	7.71 (6.8)	15.86 (4.1)
	40	9.71 (1.1)	7.90 (4.2)	7.92 (3.4)	21.67 (2.2)
	50	11.0 (0.4)	8.5 (3.0)	8.91 (3.6)	27.02 (6.1)
	75	12.6 (6.7)	10.0 (1.5)	11.0 (1.1)	55.03 (2.1)
	100	12.1 (2.4)	10.2 (4.0)	14.3 (3.4)	92.10 (1.0)
3D-TS-FRC	10	3.79 (0.9)	4.63 (5.4)	4.74 (6.5)	4.7 (8.5)
	15	5.09 (1.2)	5.41(6.5)	5.55 (4.5)	7.09 (4.2)
	20	6.12 (1.0)	5.63 (4.5)	6.36 (5.2)	9.91 (3.05)
	25	6.9 (3.0)	6.9 (1.7)	7.1 (2.0)	13.5 (2.6)
	30	8.02 (2.0)	7.43 (2.9)	7.66 (3.3)	15.41 (3.2)

	40	9.59 (1.8)	8.50 (3.0)	8.96 (3.3)	23.66 (4.1)
	50	9.4 (3.18)	7.7 (6.5)	8.8 (8.7)	34.0 (5.4)
	75	10.2 (5.9)	8.3 (1.1)	12 (1.0)	64.0 (1.8)
	100	10.7 (2.4)	11.0 (3.9)	------	100 (0.7)

3.1.2. Penetration threshold and energy profile diagram

One of the best ways to assess the impact resistance of FRC is by identifying the penetration and perforation thresholds [49]. These parameters define how much energy is required to penetrate or completely perforate the composite specimen. These thresholds are defined in an energy profile diagram (EPD). The energy profile diagram indicates the relationship between incident/impact energy and dissipated (E_a)/elastic (E_{el}) energy, perforation energy (E_{perf}) and penetration energy (E_{pene}). Fig.6(a) shows the energy profile diagram of thermoplastic and thermoset based 3D-FRCs. The experimental data were fitted in terms of impact energy versus dissipated energy curves. The difference between impact energy and dissipated energy is the elastic energy, which is the rebound energy of the impactor. At 75 J, the dissipated energy is below the equal energy line, which indicates that impactor rebounds in both 3D-FRC. The impactor on thermoplastic-based 3D-FRC rebounds with higher elastic energy, due to lower damage area, higher peak force, and less contact duration. At 100 J, the thermoset based 3D-FRC dissipated all the impact energy in the form of extensive damage and undergoes complete penetration. In the thermoplastic-based 3D-FRC, the penetration threshold was not reached at 100 J; therefore, the impactor rebounded with the remaining elastic (excess) energy.

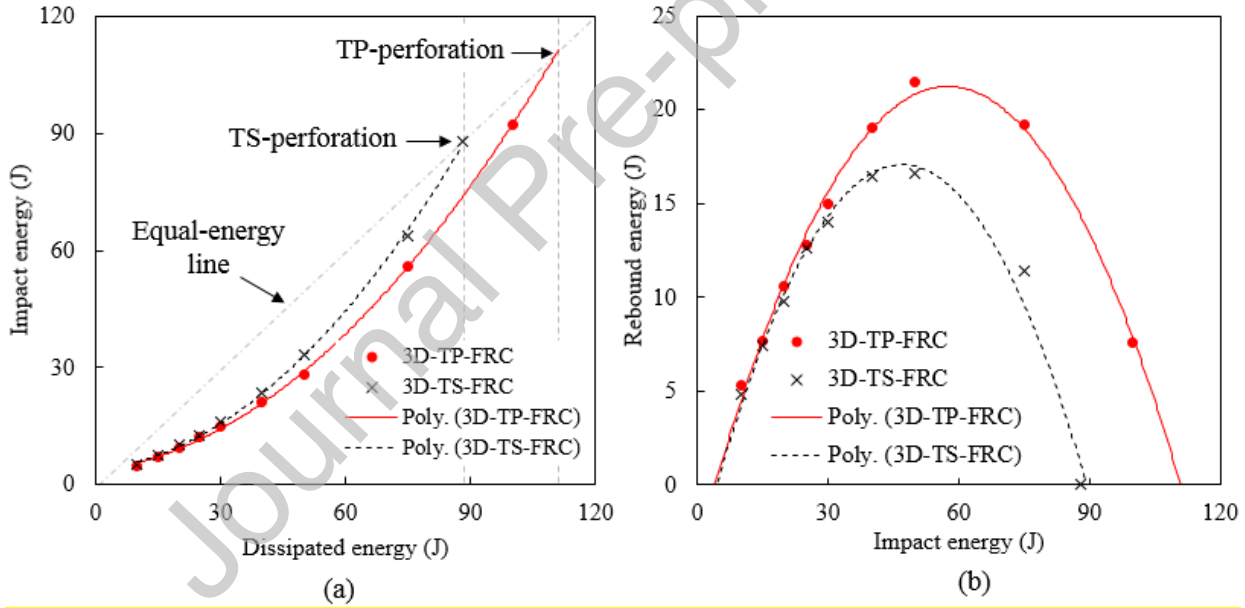

Fig.6. Effect of resin toughness on the penetration thresholds of thermoplastic and thermoset 3D composite at different impact energies. The red and black colors represent the response of thermoplastic and thermoset 3D composites, respectively. (a) impact energy vs. dissipated energy curve, and (b) impact energy vs. elastic energy curves. The impact/dissipated energy represents three main stages i.e. impact energy > dissipated energy (rebound), impact energy = dissipated energy (penetration) and impact energy > dissipated energy (perforation). Elastic energy represents the rebound energy of the indenter.

In this study, no penetration occurred in the case of thermoplastic-based 3D-FRC under a single impact load since the dissipated energy is far below the equal energy line. Fig.6(b) shows the graph between elastic/rebound energy and impact/incident energy. The thermoplastic-based 3D-FRC showed higher elastic energy at all incident energies. The graph indicates that up to 15 J of elastic energy, the impactor rebounds in both materials with the same elastic energy. In the case of thermoset based 3D-FRC, the maximum elastic energy (16.5 J) was achieved at ~ 50 J of incident energy,

whereas in the case of thermoplastic-based 3D-FRC, maximum elastic energy (22 J) was achieved at ~ 70 J of incident energy. At 75 J, rebound energy in the thermoplastic-based 3D-FRC was 41% higher than thermoset based 3D-FRC. The trend lines in the elastic/rebound energy and impact/incident energy plots highlight that the complete penetration in the thermoset and thermoplastic composites is expected to start at ~88 J and ~110 J, respectively.

3.1.3. Impact resistance of 3D-FRC under single impact

Impact resistance of FRC is one of the deciding factors in the maintenance and the design of composite structures. It is characterized based on the damaged area and permanent indentation depth in FRC at certain impact energy. In this study, the impact resistance of 3D-FRC was evaluated by comparing both indentation depth and damaged area. Fig.7. shows the damaged area in both 3D-FRC under backlight, which indicates that the damaged area increases with increasing impact energy. Fig.8(a). shows change in the damaged area in the thermoplastic and thermoset based 3D-FRCs as a function of impact energy. The error bars indicate variation in the measured damage area of three repeat specimens at each impact energy. In both cases, trend lines were added, which indicates that the damaged area in both 3D-FRCs increases linearly with impact energy. The graph highlights that thermoset based 3D-FRCs have significantly higher damage area as compared to thermoplastic-based 3D-FRC. At 50 J and 75 J, the thermoplastic-based 3D-FRC exhibited 44% and 37% less damaged area as compared to thermoset based 3D-FRC. The measured damage area in the thermoset based 3D-FRC at 50 J is 1280 mm^2, which is consistent with the damaged area measured by Kevin et al.[22] in the thermoset based 3D-FRC at 50 J, i.e., 1190 mm^2.

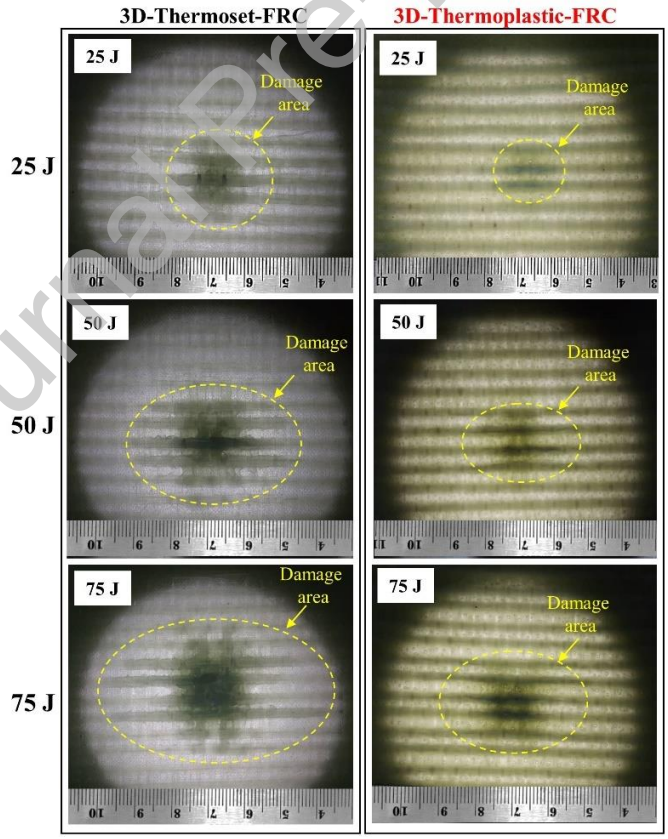

Fig.7. Comparison of damage area in thermoplastic and thermoset 3D composite under backlight at 25J, 50J, and 75J. The yellow dashed circles represent projected damage areas under the backlight.

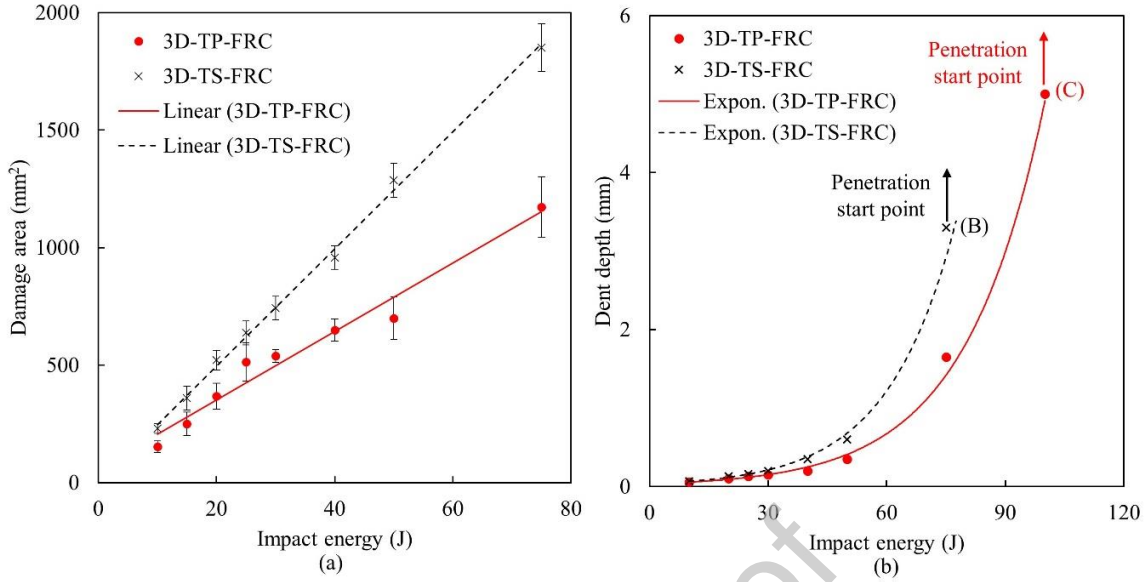

Fig.8. Impact resistance of 3D composite at different impact energies, (a) change in the damaged area as a function of impact energies. (b) change in the indentation depth in 3D-FRC as a function of impact energy on the impact face of the specimen. The red and black colors represent the response of thermoplastic and thermoset 3D composites, respectively. Point B and C represent the penetration start in thermoplastic and thermoset 3D composite.

Permanent indentation is one of the main energy absorption mechanisms in FRC, along with delamination or fiber splitting/peeling [3, 5]. The permanent indentation causes local fiber failure, delamination, and matrix plastic deformation at or near the impacted region. The permanent indentation caused by the impact indicates the extent of damage; therefore, it is essential to measure the indentation depth in FRC after an impact event. Fig.8(b). depicts the change in the indentation depth of thermoplastic and thermoset based 3D-FRC as a function of impact energy. Both 3D-FRCs highlight that the indentation depth increases exponentially as the incident energy increases. As the indentation depth increases exponentially, other macro failure mechanisms become apparent. The performance difference between the two materials also becomes visibly apparent after that, and for example, at 75 J, the thermoset based 3D-FRC showed a 3.3 mm indentation depth as compared to 1.65 mm in the case of thermoplastic-based 3D-FRC. In contrast, the thermoplastic-based 3D-FRC shows ~ 5 mm indentation depth at 100 J. The penetration of the indentor is expected to start by further increasing the incident energy in the thermoset (>75 J) and thermoplastic (>100 J) based 3D-FRC.

3.1.4. Damage characterization under single low-velocity impact

The fractography of the tested specimens gives details about damage morphologies and their extent as a function of impact energy. Fig.9. depicts the comparison of macroscopic damage at the impact face and the back face (non-impact face) of both 3D-FRCs at different low and medium impact energies. The permanent indentation caused by the hemispherical indentor on the impact face and the damage caused by the global deformation of the specimen at the bottom face is clearly visible in the macroscopic images. The damage patterns highlight that thermoplastic-based 3D-FRC exhibited significantly reduced damage at all impact energies as compared to thermoset based 3D-FRC, which was attributed to their unique failure mechanisms. The damage mechanisms have been divided into micro-damage (fiber breakage, matrix cracking, plasticization, etc.) and macro-damage (permanent indentation, debonding/delamination, z-crown failure, yarn straining, etc.) The damage mechanism observed from single LVI tests has been summarised in Table.5.

Table.5. The relative severity of damage mechanisms for changing velocity in a single low-velocity impact test for the thermoplastic and thermoset 3D composite

Material	Damage scale	Damage mechanisms	**Case-1** (25 J/3.0 ms^{-1})	**Case-2** (50 J/4.4 ms^{-1})	**Case-3** (75 J/5.4 ms^{-1})	**Case-4** (100 J/6.2 ms^{-1})
3D-TP-FRC	Micro damage	Fiber breakage	None	Some	Moderate	Moderate
		Plasticization	Dominant	Dominant	Significant	----------
		Matrix cracking	None	Some	Some	Moderate
	Macro-damage	Yarn debonding	None	None	Some	Moderate
		Z-crown failure	None	Some	Moderate	Significant
		Yarn straining	None	None	None	Significant
		Surface VID	BV	BV (>Case 1)	CV	CV
3D-TS-FRC	Micro damage	Fiber breakage	Some	Moderate	Significant	Significant
		Plasticization	None	None	None	----------
		Matrix cracking	Some	Significant	Significant	Significant
	Macro-damage	Yarn debonding	Some	Significant	Significant	Significant
		Z-crown failure	Some	Moderate	Moderate	Moderate
		Yarn straining	None	None	None	None
		Surface VID	BV (>TP)	CV	CV(>TP)	----------

VID = Visible impact damage, BV = Barely visible, CV = Clearly visible

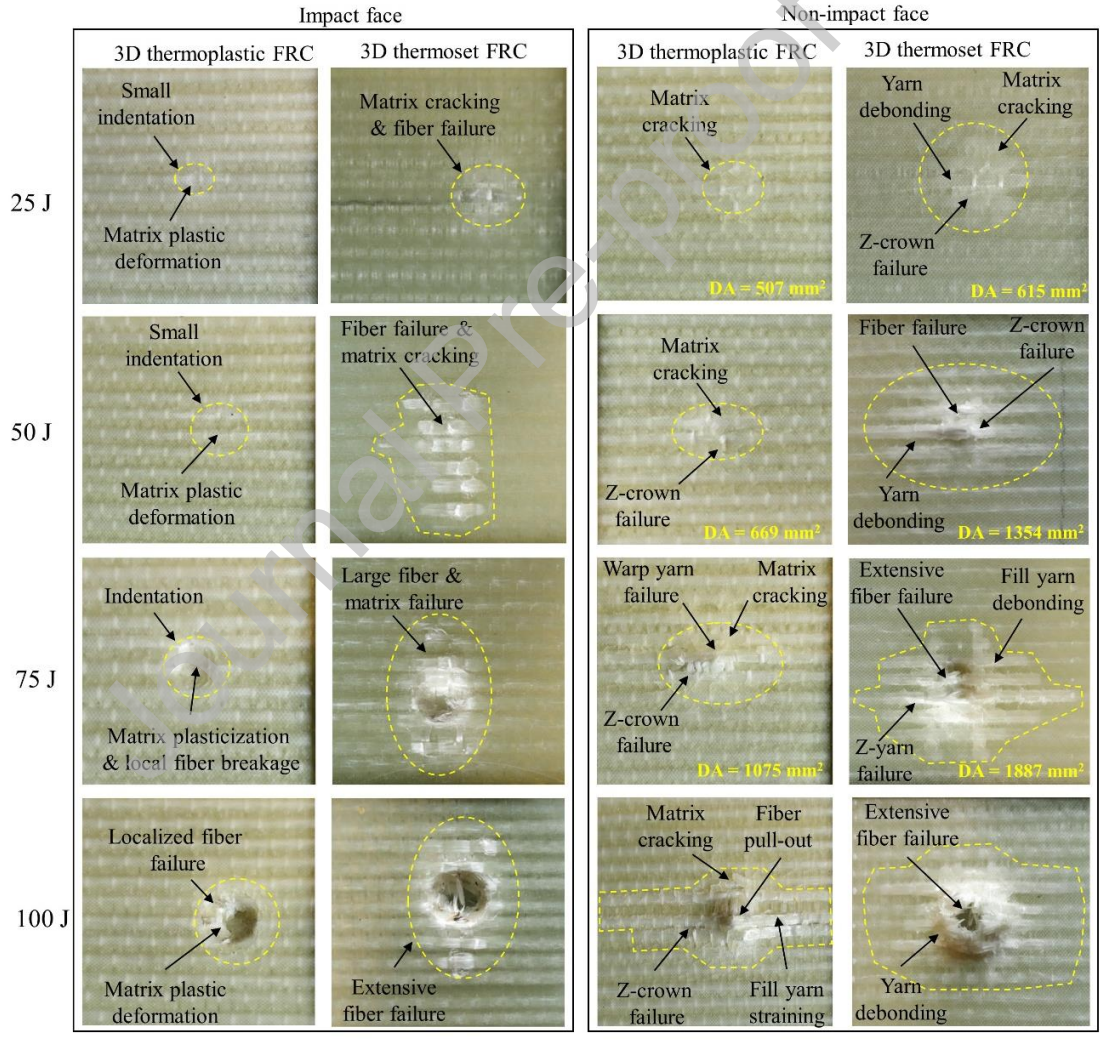

Fig.9. Comparison of macroscopic damage morphologies at the impact and non-impact face of the thermoplastic and thermoset 3D composite under a single low-velocity impact test. The damage is compared at different impact energies, i.e., 25J, 50J, 75J, and 100J. The yellow dashed regions represent damage areas at different impact energies and DA represents the calculated damaged area in each case.

As the indentor comes in contact with the surface, it produces local deformation in the form of permanent indentation on the surface of the specimen. The depth of indentation depends on the mass of the projectile and its velocity [3]. In this study, the mass of the impactor is kept constant, while the velocity was varied by changing its height. As summarized in Table.5, at low impact velocity, the indentor triggers micro-damage at the impact zone. The severity of the micro-damage depends on the matrix toughness. In the case of thermoset based 3D-FRC, it produces significant matrix cracking and large fiber/yarn damage; whereas, the thermoplastic-based 3D-FRC undergoes plasticization and slight fiber/yarn damage. In terms of macro-damage, no significant damage was observed in the thermoplastic-based 3D-FRC (Case-2). In comparison, the thermoset based 3D-FRCs undergo significant fiber/yarn breakage and z-crown failure. The results (summarized in Table.5) highlights that once the indentor velocity increases further, the surface indentation becomes clearly visible in both thermoplastic and thermoset based 3D-FRC (Case-3) due to the increase in the energy absorption. It is observed that the yarns gradually fail, and the crack propagates along the warp and fill direction, which results in the localized out-of-plane shearing of yarns at the back face of the specimen. In terms of micro-damage, the thermoplastic-based 3D-FRC shows significant plasticization at the impact face, whereas, at the back face, moderate fiber breakage and matrix cracking were identified. In comparison, the thermoset based 3D-FRC shows significant fiber breakage and matrix cracking at both faces. In terms of macro damage, the thermoplastic-based 3D-FRC undergoes significant z-crown failure and yarn straining, which dissipates all the incident energy and stops the indentor. In contrast, the thermoset based 3D-FRC shows extensive fiber/yarn failure and yarn debonding, which results in complete perforation of the projectile at 88 J (Case-4).

Fig.10. depicts damage at the back face of the specimen from a side view at different low (25 J and 50 J) and medium (75 J and 100 J) impact energies. The side view image allows for measuring the height (extension) of the damage zone. The damage extension at the bottom face increases with increasing impact energies, as expected; however, the damage extension in the thermoset based 3D-FRC is 2–3 times higher as compared to thermoplastic-based 3D-FRC. At 50 J and 75 J, the thermoplastic-based 3D-FRC showed approximately three times less damage extension on the back face.

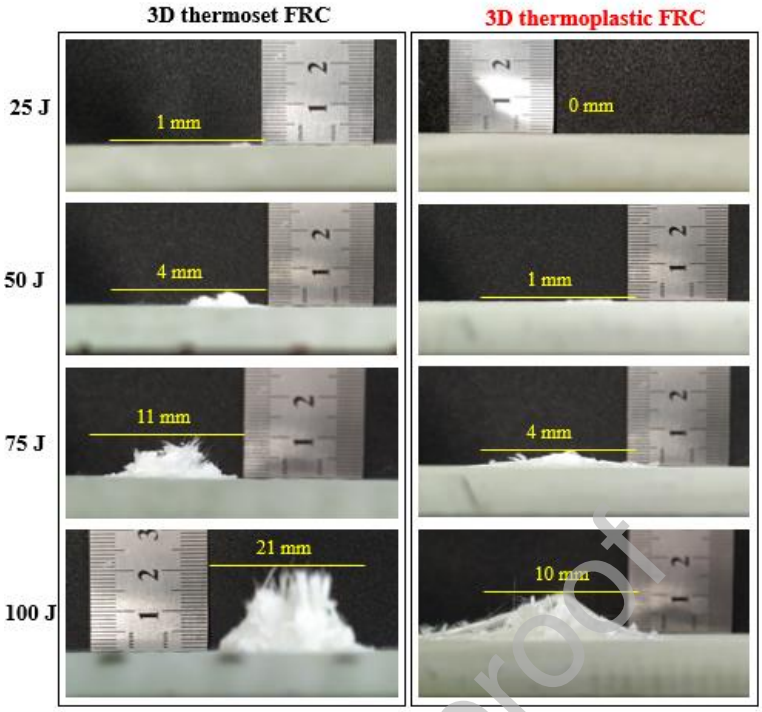

Fig.10. Comparison of damage extension at the non-impact face of thermoplastic and thermoset 3D composite at different impact energies i.e. i.e. 25J, 50J, 75J and 100J.

3.2. Recurring Strike impact test

In addition to the single impact test, recurring strike impact tests were also performed at 30 J and 50 J for up to five successive strikes (with the same incident energy), to investigate damage growth in both 3D-FRCs. After each strike, various parameters, i.e., specimen deflection, impact energy, dissipated energy, and impact force were recorded by the data acquisition system. At 30 J, both 3D-FRCs showed an almost similar impact response; for up to five successive strikes. However, at 50 J, both 3D-FRCs showed significantly different responses. The thermoplastic-based 3D-FRC sustained all five successive strikes without penetration; whereas, the thermoset-based 3D-FRC showed complete perforation at the fourth strike.

3.2.1. Force-displacement, energy-time and force-time response

Fig.11.(a) and (b) show the force-displacement curves of thermoplastic and thermoset based 3D-FRC at 50 J after five and four successive strikes, respectively. The thermoplastic-based 3D-FRC sustained all five strikes and possessed a closed curve after fifth successive strikes. In contrast, the thermoset based 3D-FRC possesses an opened curve after the fourth strike representing complete perforation of the specimen. After the first strike, the bending stiffness of both 3D-FRC was approximately the same; however, after successive strikes, both 3D-FRCs exhibited reduced bending stiffness, contact force, and slope. The force-displacement curves also indicated that the thermoplastic-based 3D-FRC has higher contact-force, bending stiffness, and lower deflection. As the number of strikes increased, bending stiffness in the thermoset based 3D-FRC degraded more rapidly as compared to thermoplastic 3D-FRC. After the third strike, the bending stiffness and deflection of thermoplastic-based 3D-FRC were reduced by 12% and 10%; in contrast, the thermoset based 3D-FRC showed 46% and 23% reduction, respectively. This indicates that the thermoset based 3D-FRC exhibited 34% lower bending stiffness and 14% higher deflection. Fig.11(c) and (d) depict force-time and energy-time curves of the thermoplastic and thermoset based 3D-FRC, respectively. After the first strike, the peak

force in the thermoplastic and thermoset based 3D-FRC were ~12.5 kN and ~11.5 kN; whereas, after the third strike the peak force reduced to ~10.6 kN and ~7.8 kN, respectively. This higher peak force represents lower damage and a higher load-bearing capacity of thermoplastic-based 3D-FRC. In terms of energy absorption, after the first strike, the thermoplastic and thermoset based 3D-FRC dissipated 32 J and 30 J of incident energy. While, after the third strike, the dissipated energy increased to 34 J and 39.5 J, respectively. After the fifth strike, the thermoplastic 3D-FRC dissipated 98% of incident energy, and the impactor rebounded due to the remaining 2% of the elastic energy. In comparison, the thermoset based 3D-FRC dissipated 70% of incident energy after the fourth strike and the impactor completely perforated the specimen. The difference between single and repeated impact, in terms of force-time response can be evaluated from Fig.11(c) and Fig.11(d), i.e., the first impact and the final impact. After each successive strike the load bearing capacity of both 3D composite decreases. However, it decreases more rapidly in the thermoset composites as compared to thermoplastic composite, due to difference in the fracture toughness and ductility of thermoplastic and thermoset matrix.

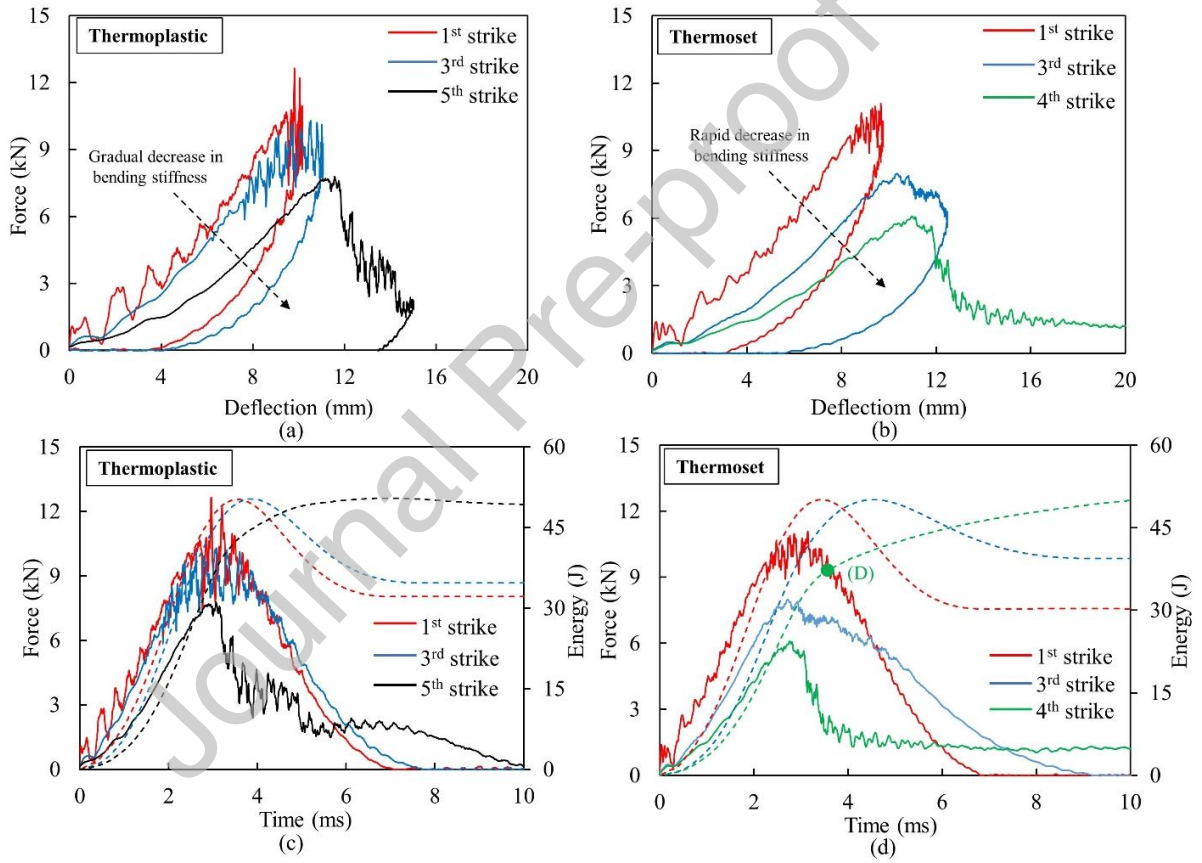

Fig.11. Comparison of the recurring low-velocity impact performance of thermoplastic and thermoset 3D composite at 50J. (a) force/displacement curves of 3D thermoplastic composites, (b) force/displacement curves of 3D thermoset composites, (c) force/time and energy/time curves of 3D thermoplastic composites, and (d) force/time and energy/time curves of 3D thermoset composites. The red, blue, green, and black colors represent the first, third, fourth, and fifth successive impact, respectively. The solid line represents force/time curves, and the dashed line represents energy/time curves. The green point "D" represents the point after which perforation starts in thermoset composite after the fourth strike.

3.2.2. Comparison of force, deflection, dissipated energy, contact time with multiple strikes

The impact performance of both 3D-FRCs under multiple strikes at 30 J and 50 J was evaluated in terms of dissipated energy, contact force, deflection, and the contract duration, as shown in Fig.12. After five successive strikes

at 30 J, there were no significant differences in the impact performance of both materials. These differences become more prominent; however, after a few more successive strikes at the same incident energy [7]. Multiple strikes at 50 J clearly highlight the effect of resin toughness on the impact performance of 3D-FRC. The thermoset based 3D composite dissipated all the impact energy for the fourth strike with a complete perforation of the specimen, as shown in Fig.12(a). Whereas, the thermoplastic-based 3D-FRC dissipated 72% of the incident energy and caused the impactor to rebound with the remaining 28% of the elastic energy. Fig.12(b) shows the contact force after each strike. On the other hand, the thermoplastic-based 3D-FRC shows a 42% higher peak force as compared to thermoset based 3D-FRC after the fourth strike. The peak deflection of a rectangular specimen after each strike is shown in Fig.12(c). Both types of 3D-FRCs possess approximately similar deflection until the second strike. Meanwhile, after the second strike, the thermoset based 3D-FRC shows an exponential increase in the peak deflection and reached the maximum value of 23.5 mm after the fourth strike. However, after the fourth strike, the thermoplastic-based 3D-FRC shows a 53% less peak deflection. In terms of contract duration, the thermoplastic-based 3D-FRC depicts 36% less contact duration after the fourth strike, as shown in Fig.12(d).

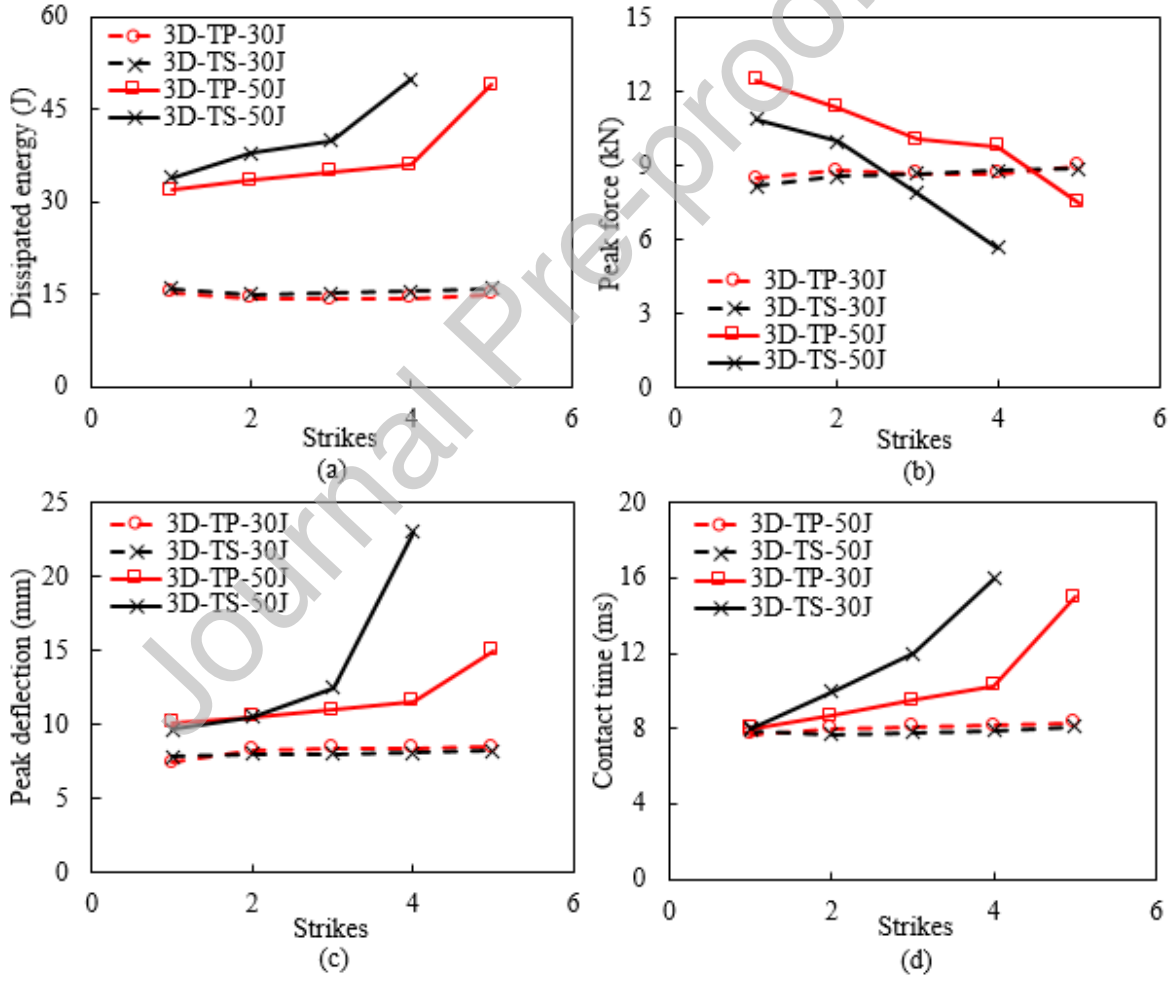

Fig.12. Comparison of thermoplastic and thermoset composite after five successive strikes at 30J and 50J. (a) dissipated energy as a function of strikes, (b) contact force as a function of strikes, (c) deflection as a function of strikes, and (d) contact time as a function of strikes. The red and black colors represent the response of thermoplastic and thermoset 3D composites, respectively. The solid line and dash line represent the response of thermoplastic and thermoset 3D composite at 50J and 30J, respectively.

3.2.3. Impact resistance of 3D-FRC under recurring strike impact

The impact resistance of 3D-FRC under recurring strike impact was determined by comparing indentation depth and damaged area of specimens after the fifth successive strike. The damaged area and indentation depth were measured through image analysis of damaged specimens and dial gauge, respectively, as discussed in section. 2.5. In the case of recurring strike impact at 30 J, the thermoplastic and thermoset based 3D-FRC showed 0.15 mm and 0.7 mm indentation depth after the fifth strike, respectively. At 50 J, the indentation depth in the thermoplastic-based 3D-FRC was increased to 6 mm after the fifth stroke, whereas in thermoset based 3D-FRC, complete perforation occurred after the fourth strike. Hence, at 50 J, the indentation depth and damaged area in the thermoset based 3D-FRC were not measured. In terms of the damaged area, the thermoplastic-based 3D-FRC showed a 50% less damage area after the fifth strike at 30J.

3.2.4. Damage characterization under recurring strike low-velocity impact

Fig.13. shows the fractography of damaged specimens after the fifth successive strike at 30 J and 50 J. The higher damage patterns in the thermoset based 3D-FRC highlights that it is more sensitive to the recurring strike impact loads. Main damage patterns in the thermoplastic-based 3D-FRC were indentation at the impact face, while matrix cracking, fiber failure, and extensive fill yarn straining at the back face (at highest impact energy). Meanwhile, the thermoset based 3D-FRC failed due to matrix cracking and extensive fiber failure at both face and fill yarn debonding at the back face of the specimen. The micro and macro damage mechanisms obtained from recurring strike LVI impact were summarized in Table.6.

Table.6. The relative severity of damage mechanisms for changing velocity in recurring low-velocity impact tests for thermoplastic and thermoset 3D composite.

Material	Damage scale	Damage mechanisms	**Case-A** (30 J/3.4 ms^{-1})	**Case-B** (50 J/4.4 ms^{-1})
3D-TP-FRC	Micro damage	Fiber breakage	Some	Moderate
		plasticization	Dominant	Significant
		Matrix cracking	Slight	Moderate
	Macro-damage	Yarn debonding	None	Moderate
		Z-crown failure	Slight	Significant
		Yarn straining	None	Significant
		Surface VID	CV	CV(>Case-A)
3D-TS-FRC	Micro damage	Fiber breakage	Moderate	Significant
		plasticization	None	None
		Matrix cracking	Moderate	Significant
	Macro-damage	Yarn debonding	Moderate	Significant
		Z-crown failure	Moderate	Moderate
		Yarn straining	None	None
		Surface VID	BV	---------

VID = Visible impact damage, BV = Barely visible, CV = Clearly visible

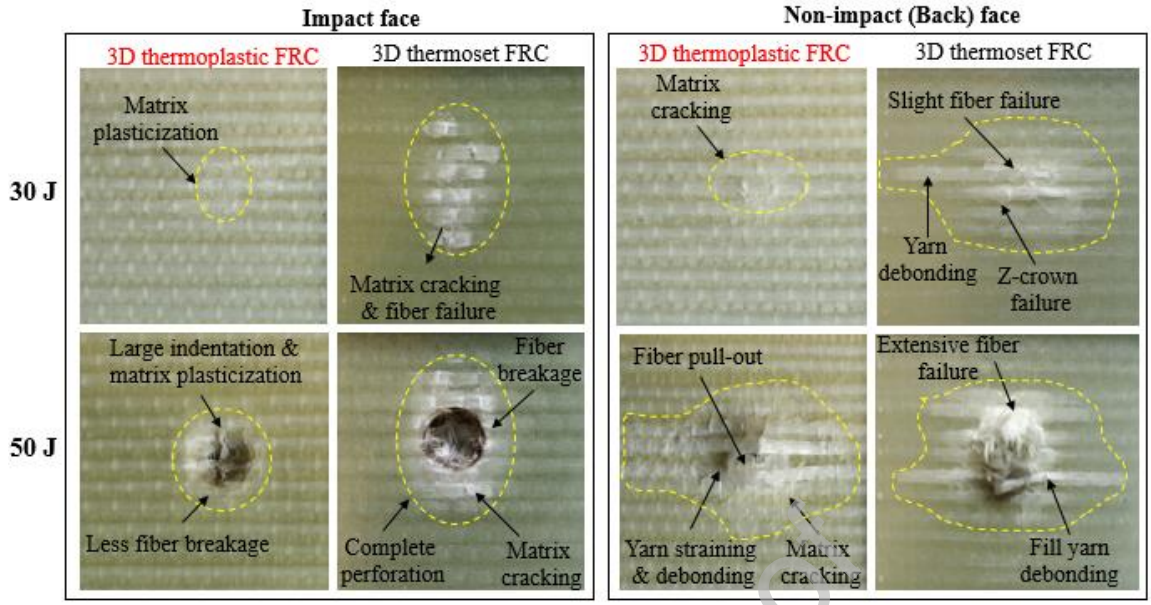

Fig.13. Comparison of macroscopic damage morphologies at the impact and non-impact face of thermoplastic and thermoset 3D composite under recurring low-velocity impact test. The damage is compared at different impact energies, i.e., 30J and 50J. The yellow dashed regions represent damage areas at different impact energies after the fifth successive strike.

The micro-damage due to recurring strike impact at 30 J shows that the thermoplastic-based 3D-FRC undergoes plasticization under the indentor at the impact face; meanwhile, slight matrix cracks were observed at the back face. In comparison, the thermoset based 3D-FRC shows fiber moderate breakage and matrix cracking (Case-A). The recurring strike impact 50 J shows significantly higher micro-damage. The thermoplastic-based 3D-FRC undergoes extensive plasticization and much-reduced fiber breakage; whereas, in the thermoset based 3D-FRC, significant fiber breakage and matrix cracking were observed (Case-B). In terms of macro-damage (30 J), the thermoplastic-based 3D-FRC depicts slight z-crown failure, which indicates that through the thickness reinforcement resist the fill yarn debonding at the back face of the specimen. In contrast, the thermoset based 3D-FRC undergoes higher yarn debonding, and z-crown failure (Case-A). Recurring strike impact at 50 J depicts much greater damage in both 3D-FRC (Case-B). The thermoplastic-based 3D-FRC shows significant yarn straining and z-crown failure, which dissipates all the energy and stops the indentor after the fifth successive strike. In contrast, the thermoset based 3D-FRC undergoes significant yarn debonding. The extensive micro and macro damage lead to the complete perforation of the impactor after the fourth successive strike. Fig.14. shows the comparison of damage extension at the back face of the specimen from a side view, after the fifth successive strike. At 30 J, the thermoplastic-based 3D-FRC showed 50% less damage extension at the bottom face; whereas, at 50 J, the damage extension in the thermoplastic (after the fifth strike) and thermoset (after the fourth strike) based 3D-FRC were 8.5 mm and 19 mm, respectively.

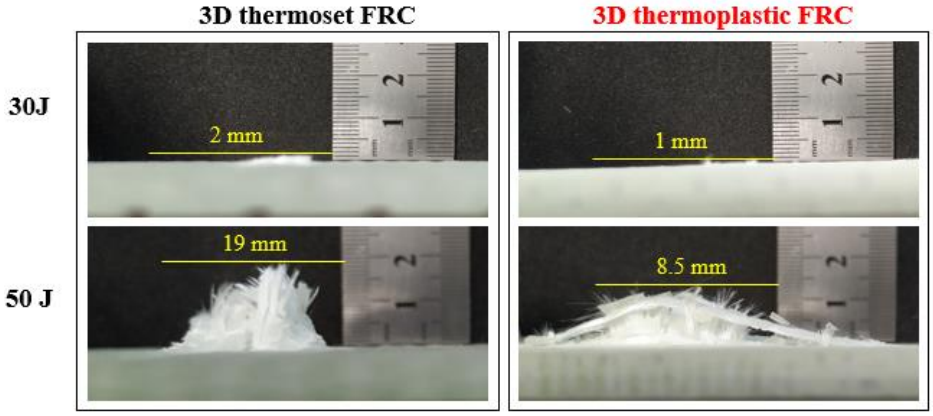

Fig.14. Comparison of damage extension at the bottom face (non-impact face) of thermoplastic and thermoset 3D composite after five successive strikes at 50J and 30J.

3.2.5. Damage accumulation under recurring strike impact

The damage accumulation during recurring impact in the thermoplastic and thermoset composites is shown in Fig.15. The damage variable increased monotonically with each recurring strike from 0 to 1. The trend lines were also added for each material to determine the damage accumulation trend. The thermoset composite exhibits a linear pattern and rapid damage accumulation, whereas, the thermoplastic composite shows the nonlinear trend and gradual damage accumulation. The thermoset composite exhibits higher damage accumulation as compared to thermoplastic composites. For example, after the third strike, in the thermoset composite, the damage variable rose to 0.64; in comparison, it reached 0.19 in the thermoplastic composites. This indicates that after the third strike, the thermoplastic composites exhibit 47% less damage accumulation. After the second, third, and fourth strike, the accumulated damages in the thermoplastic composites were 75%, 70%, and 47% less, in comparison with thermoset composite.

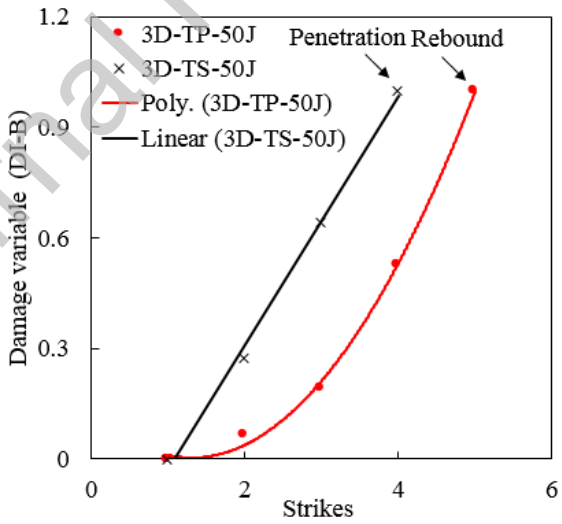

Fig.15. Comparison of damage accumulation in the thermoplastic and thermoset composite after five successive strikes at 50J. The red and black points represent damage accumulation in the thermoplastic and thermoset 3D composites. The red and black solid lines represent damage accumulation trends in the thermoplastic and thermoset 3D composites, respectively.

4. Discussion of results

Results revealed that the novel thermoplastic matrix exhibited superior impact performance under both single and recurring strike impact events. In the following section, results obtained from the impact test will be discussed in terms of impact response, damage mechanisms, and impact resistance.

4.1. Effect of the matrix on impact response of 3D-FRC

The force-displacement curves indicate that after failure initiation "F_{ini}" the bending stiffness decreases, which was attributed to matrix cracking or plasticization depending on the nature of matrix material. These matrix cracks/plasticization grow until they reach damage transition point "D_t". The damage transition point represents the transition of micro-damage (matrix cracking or plasticization) to macro-damage (delamination, yarn breakage, yarn straining, and permanent indentations). After this point, the debonding/delamination propagate until the force reaches the maximum value "F_{max}" , as shown in Fig.4(b). In the case of single impact, at low impact energies (50 J), the force-displacement curve of thermoset based 3D-FRC shows a drastic load drop (representing damage transition) (see Fig.4(b)), which was attributed to a slight penetration at the impact face of the specimen as a result of delamination/debonding propagation and extensive fiber/yarn failure at the back face of the specimen (see Fig.9). As the incident energy increases further (75 J), the damage severity increases in the form of extensive fiber breakage (see Fig.9). This behavior of the thermoset based 3D-FRC is due to a brittle epoxy matrix, which triggers matrix cracks and fiber breakage. This damage propagates rapidly after damage transition, making FRC unstable, which leads to a sudden decrease in the load. In comparison, after damage transition, the thermoplastic-based 3D-FRC undergoes plasticization and large global deformation, which significantly reduces crack propagation and fiber damage (see Fig.4(c) and (d)). This observation corroborates the finding by Bhudolia et al. [50]. Similarly, in the case of recurring strike impact, as the number of strikes increases the bending stiffness of thermoset based 3D-FRC degraded rapidly due to extensive fiber failure and unstable crack propagation leading to a complete perforation after the fourth strike (see Fig.11(b)). In contrast, the thermoplastic-based 3D-FRC sustained all five strikes and show higher load-bearing capacity (peak force) due to stronger fiber/matrix interface properties and matrix plasticization (see Fig.11(a)).

In terms of energy absorption, the thermoplastic-based 3D-FRC showed better energy absorption, which may be attributed to the plasticization of a thermoplastic matrix under the indenter. This plasticization reduces the fiber damage and cracks propagation, which results in higher energy absorption and peak force (see Fig.5(b) and (c)). In contrast, the thermoset based 3D-FRC dissipates higher energy and this extra dissipated energy results in higher damage in terms of yarn debonding, warp/fill yarns failure, and matrix cracking. In the case of a single impact, the perforation in the thermoset based 3D-FRC starts at 88 J (see Fig.5(d)), whereas, in the case of recurring strike impact (50 J), perforation starts at 35 J after the fourth strike (see Fig.11(d)). While the remaining incident energy was used during the perforation process in the form of friction between the impactor and the specimen. This friction force between the impactor and composite material completely stops the impactor, and both the incident and elastic energy becomes zero. In terms of load-bearing capacity, the thermoplastic-based 3D-FRC shows higher peak force, which was attributed to less fiber/yarn damage and plasticization of the thermoplastic-based 3D-FRC, as discussed.

These results highlight that the force-displacement, force-time, and energy-time response of both types of 3D-FRC show completely dissimilar behavior at all impact energies. The difference in the force-time and energy-time plots clearly indicate that the material response and damage mechanisms of both 3D-FRCs were significantly different. This improved performance of thermoplastic-based 3D-FRC is attributed to the strong fiber/matrix interface properties, as

discussed by Bhudolia et al.[51] and Kinvi et al.[52]. Bhudolia et al. [50] compared the interlaminar fracture toughness of Elium® and Epolam® and found that Elium® possesses 72% higher fracture toughness. Hence, higher interlaminar fracture toughness and strong fiber/matrix interface of a novel thermoplastic resin (Elium®) facilitate in reducing the crack propagation and fiber failure, which improves the impact performance of thermoplastic-based 3D-FRC. On the other hand, micro-cracks developed in the brittle epoxy matrix propagate rapidly and increase yarn debonding/delamination in the thermoset based 3D-FRC, which significantly decreases their impact performance.

In this study, no penetration occurred in the case of thermoplastic-based 3D-FRC under a single impact load since the dissipated energy is far below the equal energy line. This indicates that the penetration threshold was not reached. Whereas, in the case of thermoset based 3D-FRC at 88 J, dissipated energy is equal to the impact energy, which indicates that the penetration threshold of thermoset based 3D has been reached. These observations allow us to conclude that the penetration thresholds of the thermoset based 3D-FRC lie in between 75 J to 88 J; whereas the penetration threshold of thermoplastic-based 3D-FRC lies in between 100 J to 125 J (see Fig.6(a)). In term of perforation thresholds, the dissipated energy is higher than impact energy in the thermoset based 3D-FRC; therefore the perforation threshold is ~ 88 J. Whereas, in the case of thermoplastic-based 3D-FRC, the perforation thresholds were not measured experimentally because the maximum achievable impact energy with this setup was 100 J (5.101 kg mass and 2 meters height). However, the graph between elastic energy and rebound energy indicates that the elastic energy becomes zero at ~ 110 J, which is the penetration limit of thermoplastic-based 3D-FRC (see Fig.6(b)).

4.2. Effect of the matrix on damage mechanisms of 3D-FRC

The damage morphologies highlight that both 3D-FRC showed significantly different damage mechanisms. In FRC, impact induced-damage mechanisms depend on the properties of constituents, i.e., fiber/matrix interface strength, interlaminar fracture toughness, and matrix ductility, as well as, their energy absorption mechanisms, i.e., permanent indentation, flexural deformation, plasticization, yarns straining, fiber/yarn damage, and matrix cracking. The thermoplastic (Elium®) based 3D-FRC exhibited superior fracture toughness, fiber/matrix interface properties, and matrix ductility, which gives excellent stability and resistance against impact loads.

The 3D orthogonal fabric architecture contains matrix rich pockets on the top and bottom face due to the interlacing of fill yarns and z-binder. These resin-rich pockets play a significant role in the impact response of 3D-FRC, as they first come in contact with the indentor and produce matrix damage (cracking or plasticization). The higher fracture toughness and matrix ductility of the thermoplastic matrix allows a better stress transfer between fiber and matrix, which results in a unique energy absorption mechanism, i.e., yarn straining (only present in thermoplastic-based 3D-FRC at medium impact energies). Another important reason for this improved damage resistance of thermoplastic-based 3D-FRC is the plasticization in the thermoplastic matrix (Elium), which facilitates the absorption of additional incident energy. During the plasticization, composites dissipate incident energy through flexural deformation and through inter-laminar shear [51]. In addition to this, the thermoplastic matrix provides better stability to 3D-FRC once they are damaged, which improves their structural integrity. Finally, a strong fiber/matrix interface, which plays a major role in decreasing the fiber failure and overall severity of the damage.

It was observed that at medium impact energies (75 J and 100 J), there was no significant difference in the damage severity of thermoset based 3D-FRC (see Fig.9). This suggests that, a) the damage is velocity dominant, b) the brittle and weak fiber/matrix interface of thermoset based 3D-FRC allows for small global flexural deformation. Both these phenomenon leads to localized damage in the form of extensive fiber failure. In contrast, the thermoplastic-based

3D-FRC undergoes higher global deformation due to the toughened thermoplastic matrix, which results in significantly less fiber damage. Under both single and recurring strike impact, the thermoset based 3D-FRC exhibited ~3 times higher damage extension at the back face as compared to thermoplastic-based 3D-FRC (see Fig.10 and Fig.14). This higher damage extension in thermoset based 3D-FRC was attributed to the brittle epoxy matrix and weak fiber/matrix interface properties, which made yarns unstable in the impact zone and transferred all the impact load to fiber/yarns. Such higher damage extension for thermoset based 3D-FRC was also reported by Umer et al. [26]. Whereas, the plasticization and strong fiber/matrix interface reduce damage extension in the thermoplastic-based 3D-FRC. Therefore, the thermoplastic-based 3D-FRC exhibited significantly higher damage resistance at all impact energies investigated in this study.

It is important to understand the role of z-binder and matrix toughness in dissipating higher impact energy in 3D-FRC. The z-binder, binds the in-plane warp and fill yarn and reduces delamination by increasing interlaminar shear strength and crack bridging under impact loads [22]. In the thermoplastic-based 3D-FRC, z-crown failure starts near the impact region and travels outward towards the outer boundaries [53]. This progressive failure of z-crown in the thermoplastic-based 3D-FRC introduces a straining effect in the fill yarns (see Fig.9. and Fig.13.). It was observed that fill yarns were detached from the boundaries and start sliding through z-crown. This damage mechanism dissipates a large amount of energy in the form of frictional sliding of fill yarn through the z-crowns and fiber pull-out, which stopped the indentor earlier. In addition to this, the out-of-plane shearing of yarns at the back face of the specimen dissipates additional energy and facilitates in reducing damage severity. Hence, extensive yarn straining, out-of-plane shearing of yarns, and plasticization are the prime energy absorption mechanisms of thermoplastic-based 3D-FRC, which were not present in thermoset based 3D-FRC. Hence, the combined effect of through the thickness reinforcement and toughened thermoplastic matrix gives added stability to thermoplastic-based 3D-FRC against single and recurring impact.

The superior impact resistance of the thermoplastic based 3D composite under single and recurring LVI is due to a difference in the energy absorption mechanisms of both 3D composites, as shown in Fig.16. In the thermoplastic-based 3D composite, the primary failure mechanisms are matrix plasticization and straining of a whole yarn (see Fig.16(a)), whereas, in thermoset based 3D composite, they are matrix cracking and straining of individual fibers (see Fig.16(b)). This unique failure mechanism of a whole yarn straining in the thermoplastic composite is attributed to higher matrix ductility, which gives yarns better stability and significantly reduces the amount of damage caused by the impact (see Fig. 9, Fig 10 and Fig 16(a)). In comparison, during the straining process of an individual fiber in the thermoset based 3D composites, fibers in the yarn (warp, fill and z-yarn) start to break and move outward at the back of the specimen (see Fig. 9, Fig 10 and Fig.16(b)). This breakage and straining of individual fiber in the yarns are due to a brittle epoxy matrix, which makes yarn unstable and results in an extensive fiber failure in the form of a large damaged area at the back face of the specimen.

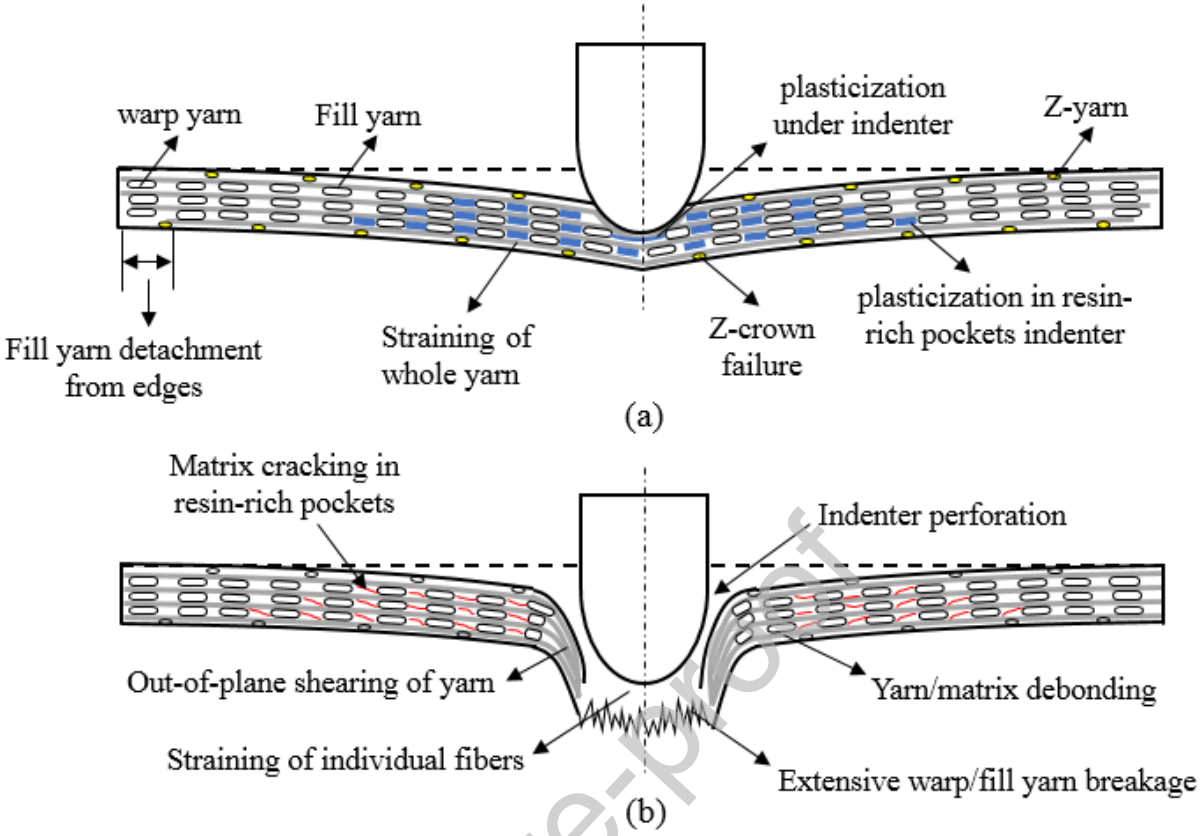

Fig.16. Schematic illustration of the failure mechanisms in 3D-FRC under low velocity impact. (a) thermoplastic 3D-FRC and (b) thermoset 3D-FRC. The dashed line represents undeformed specimen; whereas, solid line shows deformed specimen due to LVI. The blue, yellow and red colour represents matrix plasticization, z-corwn failure and matrix cracking.

4.3. Effect of matrix toughness on the impact resistance of 3D-FRC

The damage mechanisms discussed above result in damage area and permanent indentation, which describes the impact resistance of FRC. In both single and recurring strike impact events, the thermoplastic-based 3D-FRC exhibited significantly higher impact resistance. The main properties contributing to the higher impact resistance of thermoplastic-based 3D-FRC are interlaminar fracture toughness and surface hardness. Table.1. shows the comparison between the mechanical properties of Elium® and Epolam®. The thermoplastic matrix possesses ~ 3 times higher fracture toughness and ~ 20% lower surface hardness. The thermoset based 3D FRC dissipates higher incident energy, which results in greater damage in the form of fiber/matrix failure and yarn debonding (see Fig.7 and Fig.8(a)). The micro-cracks developed in the thermoset based 3D-FRC propagates rapidly in an unstable manner due to lower fracture toughness, which reveals that the thermoset based 3D-FRC is sensitive to the impact load. On the other hand, higher interlaminar fracture toughness of the thermoplastic matrix prevents yarns from opening in Mode-I and slows down the propagation of cracks, which ultimately reduces the delamination/debonding and damage area under impact event. This higher interlaminar fracture toughness and ductility make thermoplastic-based 3D-FRC less sensitive to the impact load. At all impact energies, the thermoplastic-based 3D-FRC depicts ~ 50% reduced damage area as compared to thermoset based 3D-FRC. In terms of permanent indentation under LVI, the thermoset based 3D-FRC shows higher permanent indentations at all impact energies despite higher surface hardness (> ~ 20%). This was attributed to higher damage in the form of fiber and matrix failure under the indentor (see Fig.8(b)). Another reason for this reduced permanent

indentation in thermoplastic-based 3D-FRC may be due to the presence of fiber bridging, which reduces damage extension in thermoplastic composites [5]. In contrast, in this study, the reduced permanent indentation depth in the thermoplastic-based 3D-FRC is attributed to their higher matrix toughness and plasticization under the indentor.

4.4. Damage accumulation in 3D-FRC under recurring impact

The damage which accumulates after each recurring strike results in the reduction of bending stiffness of both 3D composites (See. Fig.11(a) and Fig.11(b)). The damage accumulates in the form of matrix cracking for the thermoset matrix and combination of plasticization and matrix cracking for the thermoplastic matrix. In addition, both composites accrue fiber damage to a varying extent. Damage also grows in terms of delamination; however, it is limited in extent due to the presence of through the thickness reinforcement. The damage variable (DI-B) allows us to quantitatively compare the effect of all these separate damage mechanisms. Thus, after the third strike, the thermoplastic composite shows up to 64% less stiffness reduction as compared to thermoset composites at 50J (see Fig.11(a) and Fig.11(b)). This higher stiffness reduction in the thermoset composite is due to extensive matrix cracking and fiber breakage with each recurring strike (see Fig.15). This phenomenon is reflected by the rapid increase in the damage variable, indicating accelerated damage accumulation. In contrast, small stiffness reduction of thermoplastic composites after the first few strikes is attributed to the matrix plasticization, which reduces fiber breakage. This gradual increase in the damage variable (see Fig.15) of the thermoplastic composites results in less damage accumulation. Also, at 50J in thermoplastic composites, the difference in the damage accumulation decreases with each successive strike due to the transition of damage from matrix failure (plasticization) to fiber breakage. The fiber breakage led to a rapid increase in the damage accumulation (damage variable) after the third strike, as shown in Fig.15. After the fifth strike at 30J, the accumulated damage is mainly due to matrix plasticization/cracking, as there is no significant fiber breakage. Hence, the accumulation of damage variable allows us to quantitatively compare the improvement in impact resistance, in the case of recurring impact for the thermoplastic resin.

4.5. Comparison between single and repeated LVI

In this section, absorbed energy during single and repeated LVI has been compared to establish a relationship between them. This can be used to establish a criterion for a safe number of repeated impacts, that 3D composite can sustain without penetration for a given impact energy. The experimental results of repeated LVI shows that, the cumulative absorbed energy after fourth impact at 50J is E_a = 136J and this is sufficient to cause penetration for the thermoset composite. The theoretical cumulative absorbed energy of four single impacts at 50J (E_a = 30x4) however is 120J. This is clearly lower than the measured cumulative absorbed energy for the repeated LVI, however it is higher than the perforation threshold of 85-90J determined from the single impact tests. Thus, it can be seen that the composite can absorb overall a higher amount of energy before penetration for the repeated LVI case. The same trend holds for the 50J thermoplastic repeat LVI case and for the 30J repeat LVI case in which penetration was not observed for the five repeats used in this study. A design criterion that the minimum safe number of repeated LVI events (N_s) (i.e. without full penetration) for both thermoset and thermoplastic composites may simply be determined using the penetration threshold energy of the single LVI case and comparing that with the theoretically cumulative absorbed energy at particular impact. Thus,

$$N_s = \frac{Ea_{pt}}{Ea_i} \quad (2)$$

Where, Ea_{pt} is penetration threshold energy determined from single LVI tests (Fig. 6 and Table 4) and Ea_i is the absorbed energy for the i^{th} single impact case (Table 4) for which the minimum safe number of repeats (N_s) is to be determined. Although, in this study we did not test all specimens to perforation for the repeated LVI case the data presented is sufficient to accept this as a conservative criterion. More extensive repeated LVI testing will be required to determine a less conservative estimate and to quantitatively establish the advantage gained by using the thermoplastic composite for the repeated LVI events. Fig. 17 below shows the safe number of repeats established from equation (2) against the impact energy for both thermoset and thermoplastic composites it also shows that the minimum safe number of repeats increase following a power law behavior with the reduced impact energy.

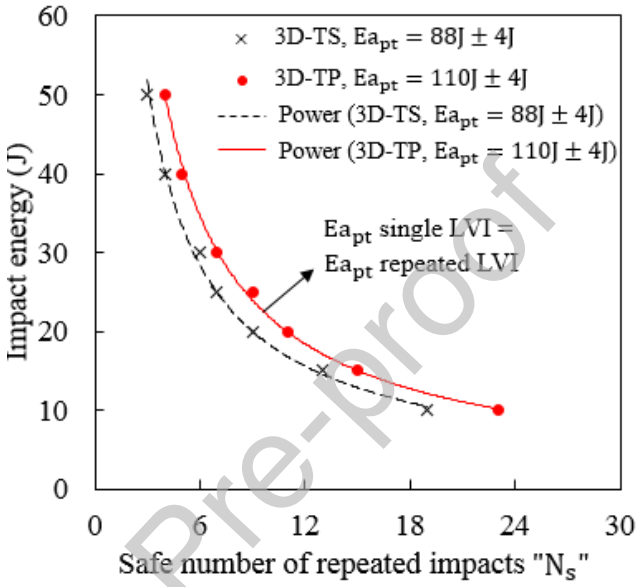

Fig.17. Comparison between single and repeated low velocity impact. Energy absorbed during single impact upto penetration = Theoretically cummulative energy absorbed during repeated impacts at (10J, 15J, 20J, 25J, 30J,40J and 50J). X-axis shows the safe number of repeated impact at different impact energies. The red and black points represent safe number of impacts in the thermoplastic and thermoset composites. The red solid line and black dashed lines represents safe number of repeated impact trends in the thermoplastic and thermoset 3D composites, respectively.

5. Conclusion

In this research work, the impact performance of thermoplastic-based 3D-FRC was explored under a single as well as recurring strike impact and compared with the thermoset based 3D-FRC. From the experimental study, the following conclusion can be drawn:

- In the case of a single impact test, the thermoset based 3D-FRC specimen is completely perforated at 88 J; whereas, the thermoplastic-based 3D-FRC caused the impactor to rebound with the remaining elastic energy. The thermoplastic-based 3D-FRC showed ~44% less damage area and ~3 times less damage extension, ~27% higher damage transition energy, and ~20% higher load-bearing capacity (peak force) in comparison with thermoset based 3D-FRC.
- In the case of a recurring strike impact test at 50 J, the thermoplastic-based 3D-FRC fully sustained all fives strikes without penetration, whereas the thermoset based 3D-FRC completely perforate after the fourth strike. After the fourth strike, the thermoplastic-based 3D-FRC showed ~42% higher load-bearing capacity (peak force), ~53% less peak defection, and ~36% less contact duration. In addition to this, the thermoplastic-based 3D-FRC exhibited ~50% less damage area and damage extension at the bottom face of the specimen. Hence,

the thermoplastic-based 3D-FRC survived more strikes and possessed superior impact resistance than thermoset based 3D-FRC under recurring strike impact.

- This confined damage area under single and recurring strike impact in the thermoplastic-based 3D-FRC is attributed to higher interlaminar fracture toughness, crack resistance, and matrix ductility, which suppresses damage propagation and increases the energy required for damage transition. Whereas, the thermoset based 3D-FRC facilitates micro-cracks to propagate rapidly, which results in higher damage.
- The main damage patterns in the thermoplastic-based 3D-FRC were indentation due to plastic deformation and slight fiber failure at the impact face of the specimen; whereas, at the back face, matrix cracking, fill yarn failure along with extensive fiber pull-out and fill yarn straining (at highest impact energy) were observed. This extensive yarn straining and frictional sliding of surface fill yarn through z-crown is the prime energy absorption mode of thermoplastic-based 3D-FRC, which were not present in thermoset based 3D-FRC. In the case of thermoset based 3D-FRC, extensive fiber failure, matrix cracking, fill yarn debonding, and complete perforation were observed.

These results revealed that the thermoplastic-based 3D-FRC exhibited much higher impact resistance and lower loss in the structural integrity under both single and recurring strike impact loads. This suggests that the novel thermoplastic-based 3D-FRC is a suitable replacement to a conventional thermoset based 3D-FRC for the aerospace industry.

Acknowledgments

The authors would like to acknowledge the financial support provided by Universiti Teknologi PETRONAS (grant number 015LC0-197). The authors would also like to acknowledge the support of Dr. Mohamed Thariq Bin Hameed Sultan from *Universiti Putra Malaysia* in providing the facility to conduct impact tests at their facility. The authors are grateful to Barsotti Robert from Arkema in providing Elium resin for this research work.

Conflicts of interest

The authors declare no conflict of interest with respect to the research or publication of this work.

References.

[1] Sarasini F, Tirillo J, D Altilia S, Valente T, Santulli C, Touchard F, et al. Damage tolerance of carbon/flax hybrid composites subjected to low velocity impact. Composites Part B: Engineering. 2016;91:144-53.

[2] Maio L, Monaco E, Ricci F, Lecce L. Simulation of low velocity impact on composite laminates with progressive failure analysis. Composite Structures. 2013;103:75-85.

[3] Choudhry RS, Hassan SF, Li S, Day R. Damage in single lap joints of woven fabric reinforced polymeric composites subjected to transverse impact loading. International Journal of Impact Engineering. 2015;80:76-93.

[4] Sutcliffe M, Aceves CM, Stronge W, Choudhry R, Scott A. Moderate speed impact damage to 2D braided glass/carbon composites. Composite Structures. 2012;94(5):1781-92.

[5] Vieille B, Casado VM, Bouvet C. About the impact behavior of woven ply carbon fiber reinforced thermoplastic and thermosetting composites: a comparative study. Composite structures. 2013;101:9-21.

[6] Baucom J, Zikry Ma, Rajendran A. Low velocity impact damage accumulation in woven S2 glass composite systems. Composites science and technology. 2006;66(10):1229-38.

[7] Atas C, Dogan A. An experimental investigation on the repeated impact response of glass/epoxy composites subjected to thermal ageing. Composites Part B: Engineering. 2015;75:127-34.

[8] Santos RAM, Reis PNB, Silva FGA, Moura MFSF. Influence of inclined holes on the impact strength of CFRP composites. Composite Structures. 2017;172:130-6.
[9] Richardson M, Wisheart M. Review of low-velocity impact properties of composite materials. Composites Part A: Applied Science and Manufacturing. 1996;27(12):1123-31.
[10] Tan W, Falzon BG, Chiu LN, Price M. Predicting low velocity impact damage and Compression After Impact (CAI) behaviour of composite laminates. Composites Part A: Applied Science and Manufacturing. 2015;71:212-26.
[11] Choudhry RS, Rhead AT, Nielsen MW, Butler R. A plate model for compressive strength prediction of delaminated composites. Composite Structures. 2019;210:509-17.
[12] He W, Lu S, Yi K, Wang S, Sun G, Hu Z. Residual flexural properties of CFRP sandwich structures with aluminum honeycomb cores after low-velocity impact. International Journal of Mechanical Sciences. 2019;161:105026.
[13] Cantwell W, Morton J. The impact resistance of composite materials: A review. Composite Materials. 1991;22(5):347-62.
[14] Wisnom M. The role of delamination in failure of fibre-reinforced composites. Philosophical Transactions of the Royal Society A. 2012;370:1850-70.
[15] Dutton S, Kelly D, Baker A. Composite materials for aircraft structures: American Institute of Aeronautics and Astronautics; 2004.
[16] Greve L, Pickett A. Delamination testing and modelling for composite crash simulation. Composites science and technology. 2006;66(6):816-26.
[17] Francesconi L, Aymerich F. Numerical simulation of the effect of stitching on the delamination resistance of laminated composites subjected to low-velocity impact. Composite Structures. 2017;159:110-20.
[18] Yasaee M, Bigg L, Mohamed G, Hallett SR. Influence of Z pin embedded length on the interlaminar traction response of multi-directional composite laminates. Materials & Design. 2017;115:26-36.
[19] He W, Liu J, Wang S, Xie D. Low-velocity impact response and post-impact flexural behaviour of composite sandwich structures with corrugated cores. Composite Structures. 2018;189:37-53.
[20] Bandaru AK, Chavan VV, Ahmad S, Alagirusamy R, Bhatnagar N. Low velocity impact response of 2D and 3D Kevlar/polypropylene composites. International Journal of Impact Engineering. 2016;93:136-43.
[21] Bandaru AK, Patel S, Sachan Y, Alagirusamy R, Bhatnagar N, Ahmad S. Low velocity impact response of 3D angle-interlock Kevlar/basalt reinforced polypropylene composites. Materials & Design. 2016;105:323-32.
[22] Hart KR, Chia PXL, Sheridan LE, Wetzel ED, Sottos NR, White SR. Mechanisms and characterization of impact damage in 2D and 3D woven fiber-reinforced composites. Composites Part A: Applied Science and Manufacturing. 2017;101:432-43.
[23] Santiago R, Cantwell W, Alves M. Impact on thermoplastic fibre-metal laminates: Experimental observations. Composite Structures. 2017;159:800-17.
[24] Shah S, Karuppanan S, Megat-Yusoff P, Sajid Z. Impact resistance and damage tolerance of fiber reinforced composites: A review. Composite Structures. 2019;217:100-21.
[25] Mahmood A, Wang X, Zhou C. Generic stiffness model for 3D woven orthogonal hybrid composites. Aerospace Science Technology. 2013;31(1):42-52.
[26] Umer R, Alhussein H, Zhou J, Cantwell W. The mechanical properties of 3D woven composites. Journal of Composite Materials. 2017;51(12):1703-16.
[27] Wang M, Cao M, Wang H, Siddique A, Gu B, Sun B. Drop weight impact behaviors of 3D angle interlock woven composites after thermal oxidative aging. Composite Structures. 2017;166:239-55.

[28] Potluri P, Hogg P, Arshad M, Jetavat D, Jamshidi P. Influence of fibre architecture on impact damage tolerance in 3D woven composites. Applied Composite Materials. 2012;19(5):799-812.
[29] Seltzer R, Gonzalez C, Munoz R, LLorca J, Blanco Varela T. X-ray microtomography analysis of the damage micromechanisms in 3D woven composites under low-velocity impact. Composites Part A: Applied Science and Manufacturing. 2013;45:49-60.
[30] Zhang D, Sun Y, Chen L, Pan N. A comparative study on low-velocity impact response of fabric composite laminates. Materials & Design. 2013;50:750-6.
[31] Zhang D, Zheng X, Wang Z, Wu T, Sohail A. Effects of braiding architectures on damage resistance and damage tolerance behaviors of 3D braided composites. Composite Structures. 2020;232.
[32] Kazemianfar B, Esmaeeli M, Nami MR. Response of 3D woven composites under low velocity impact with different impactor geometries. Aerospace Science and Technology. 2020:105849.
[33] Mouritz AP, Bannister MK, Falzon P, Leong K. Review of applications for advanced three-dimensional fibre textile composites. Composites Part A: applied science and manufacturing. 1999;30(12):1445-61.
[34] Ali M, Umer R, Khan K, Bickerton S, Cantwell W. Non destructive evaluation of through thickness permeability in 3D woven fabrics for composite fan blade applications. Aerospace Science and Technology. 2018;82:520-33.
[35] Kuo WS, Jiunn F. Processing and characterization of 3D woven and braided thermoplastic composites. Composites science and technology. 2000;60(5):643-56.
[36] Wakeman MD, Cain TA, Rudd CD, Brooks R, Long AC. Compression moulding of Glass and polypropylene composites for optimised macro and micro mechanical properties. 1998;58:1879-998.
[37] Boufaida Z, Farge L, André S, Meshaka Y. Influence of the fiber/matrix strength on the mechanical properties of a glass fiber/thermoplastic-matrix plain weave fabric composite. Composites Part A: Applied Science and Manufacturing. 2015;75:28-38.
[38] Kinvi-Dossou G, Matadi Boumbimba R, Bonfoh N, Koutsawa Y, Eccli D, Gerard P. A numerical homogenization of E-glass/acrylic woven composite laminates: Application to low velocity impact. Composite Structures. 2018;200:540-54.
[39] Obande W, Mamalis D, Ray D, Yang L, O Bradaigh CM. Mechanical and thermomechanical characterisation of vacuum-infused thermoplastic and thermoset-based composites. Materials & Design. 2019;175:107828.
[40] Chilali A, Zouari W, Assarar M, Kebir H, Ayad R. Analysis of the mechanical behaviour of flax and glass fabrics-reinforced thermoplastic and thermoset resins. Journal of Reinforced Plastics and Composites. 2016;35(16):1217-32.
[41] Bhudolia SK, Perrotey P, Joshi SC. Optimizing polymer infusion process for thin ply textile composites with novel matrix system. Materials. 2017;10(3):293.
[42] ASTM D7136 / D7136M-05, Standard Test Method for Measuring the Damage Resistance of a Fiber-Reinforced Polymer Matrix Composite to a Drop-Weight Impact Event, ASTM International, West Conshohocken, PA. 2005.
[43] Schneider C, Rasband W, Eliceiri K. NIH image to ImageJ: 25 years of image analysis. 2012;9:671-5.
[44] Abdallah EA, Bouvet C, Rivallant S, Broll B, Barrau JJ. Experimental analysis of damage creation and permanent indentation on highly oriented plates. Composites Science and Technology. 2009;69(7-8):1238-45.
[45] Belingardi G, Cavatorta MP, Paolino DS. A new damage index to monitor the range of the penetration process in thick laminates. Composites science and technology. 2008;68(13):2646-52.

[46] Liao B, Zhou J, Li Y, Wang P, Xi L, Gao R, et al. Damage accumulation mechanism of composite laminates subjected to repeated low velocity impacts. International Journal of Mechanical Sciences. 2020;182.
[47] Belingardi G, Vadori R. Low velocity impact tests of laminate glass fiber epoxy matrix composite material plates. International Journal of Impact Engineering. 2002;27(2):213-29.
[48] Hufenbach W, Gude M, Ebert C, Zscheyge M, Hornig A. Strain rate dependent low velocity impact response of layerwise 3D-reinforced composite structures. International Journal of Impact Engineering. 2011;38(5):358-68.
[49] Aktas M, Atas C, İcten BM, Karakuzu R. An experimental investigation of the impact response of composite laminates. Composite Structures. 2009;87(4):307-13.
[50] Bhudolia SK, Perrotey P, Joshi SC. Mode I fracture toughness and fractographic investigation of carbon fibre composites with liquid Methylmethacrylate thermoplastic matrix. Composites Part B: Engineering. 2018;134:246-53.
[51] Bhudolia SK, Joshi SC. Low-velocity impact response of carbon fibre composites with novel liquid Methylmethacrylate thermoplastic matrix. Composite Structures. 2018;203:696-708.
[52] Kinvi Dossou G, Matadi Boumbimba R, Bonfoh N, Garzon Hernandez S, Garcia Gonzalez D, Gerard P, et al. Innovative acrylic thermoplastic composites versus conventional composites: Improving the impact performances. Composite Structures. 2019;217:1-13.
[53] Baucom JN, Zikry M. Evolution of failure mechanisms in 2D and 3D woven composite systems under quasi-static perforation. Journal of composite materials. 2003;37(18):1651-74.

Declaration of interests

☒ The authors declare that they have no known competing financial interests or personal relationships that could have appeared to influence the work reported in this paper.

CRediT author statement

Syed Zulfiqar Hussain Shah: Conceptualization, Methodology, Formal analysis, Investigation, Visualization, Writing - Original Draft
Puteri Sri Melor Megat-Yusoff: Supervision, Investigation, Project administration, Funding acquisition.
Saravanan Karuppanan: Supervision, Investigation, Writing- Reviewing and Editing
Rizwan Saeed Choudhry: Supervision, Methodology, Formal analysis, Writing - Original Draft, Writing- Reviewing and Editing
Faiz Ahmad: Funding acquisition, Resources
Zubair Sajid: Resources
Pierre Gerard: Resources
Keith Sharp: Resources, Writing- Reviewing and Editing

Graphical Abstract

Graphical Abstract: